



**EFFECT OF ELECTRODEPOSITION CURRENT DENSITY AND
SODIUM DODECYL SULPHATE SURFACTANT (SDS) ON THE
PROPERTIES OF NICKEL-RECYCLED QUARRY DUST
COMPOSITE COATINGS**

This report is handed over in accordance with the requirements of the Universiti Teknikal Malaysia Melaka (UTeM) for the Bachelor of Manufacturing Engineering (Hons.)

اونيور سيتي تيكنيكل مليسيا ملاك
by
UNIVERSITI TEKNIKAL MALAYSIA MELAKA

MUHAMMAD ASLAM BIN ABDUL ASMIN

B052010063

010909-07-0051

FACULTY OF INDUSTRIAL AND MANUFACTURING
TECHNOLOGY AND ENGINEERING

2024

BORANG PENGESAHAN STATUS LAPORAN PROJEK SARJANA MUDA

Tajuk: **EFFECT OF ELECTRODEPOSITION CURRENT DENSITY AND SODIUM DODECYL SULPHATE SURFACTANT (SDS) ON THE PROPERTIES OF NICKEL-RECYCLED QUARRY DUST COMPOSITE COATINGS**

Sesi Pengajian: **2023/2024 Semester 2**


Saya **MUHAMMAD ASLAM BIN ABDUL ASMIN (010909-07-0051)**


mengaku membenarkan Laporan Projek Sarjana Muda (PSM) ini disimpan di Perpustakaan Universiti Teknikal Malaysia Melaka (UTeM) dengan syarat-syarat kegunaan seperti berikut:

1. Laporan PSM adalah hak milik Universiti Teknikal Malaysia Melaka dan penulis.
2. Perpustakaan Universiti Teknikal Malaysia Melaka dibenarkan membuat salinan untuk tujuan pengajian sahaja dengan izin penulis.
3. Perpustakaan dibenarkan membuat salinan laporan PSM ini sebagai bahan pertukaran antara institusi pengajian tinggi.

- SULIT** (Mengandungi maklumat yang berdarjah keselamatan atau kepentingan Malaysiasebagaimana yang termaktub dalam AKTA RAHSIA RASMI 1972)
- TERHAD** (Mengandungi maklumat TERHAD yang telah ditentukan oleh organisasi/ badan di mana penyelidikan dijalankan)
- TIDAK TERHAD**

Disahkan oleh:


Alamat Tetap:
No.3, Lorong Alma Jaya 3,
Taman Alma Jaya,
14000 Bukit Mertajam, Pulau Pinang
Tarikh: 14 JULAI 2024


Cop Rasmi: **DR. INTAN SHARHIDA BINTI OTHMAN**
Pensyarah Kanan
Fakulti Kejuruteraan Pembuatan
Universiti Teknikal Malaysia Melaka

Tarikh: 14 JULAI 2024

*Jika Laporan PSM ini SULIT atau TERHAD, sila lampirkan surat daripada pihak berkuasa/organisasi berkenaan dengan menyatakan sekali sebab dan tempoh laporan PSM ini perlu dikelaskan sebagai SULIT atau TERHAD.

DECLARATION

I hereby, declared this report entitled “Effect of Electrodeposition Current Density and Sodium Dodecyl Sulphate Surfactant (SDS) on the Properties of Ni-Recycled Quarry Dust Composite Coatings” is the result of my own research except as cited in references.

Signature

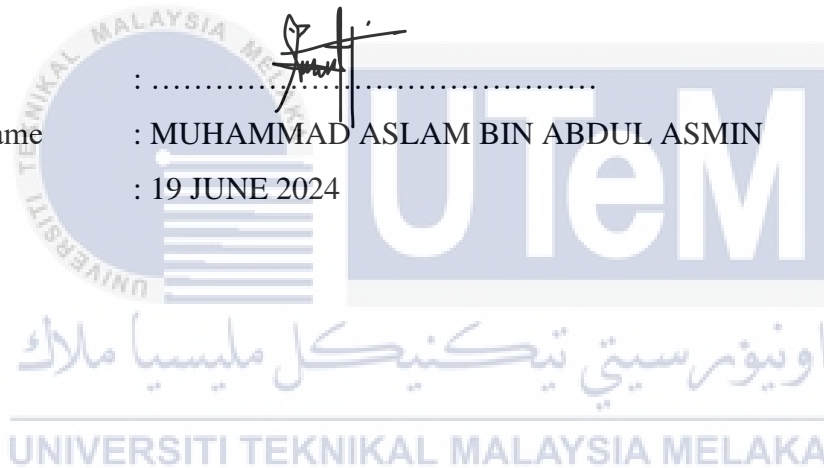
:

Author's Name

: MUHAMMAD ASLAM BIN ABDUL ASMIN

Date

: 19 JUNE 2024



APPROVAL

This report is submitted to the Faculty of Industrial and Manufacturing
Technology and Engineering
of Universiti Teknikal Malaysia Melaka as a partial fulfilment of the requirement for
Degree of Manufacturing Engineering (Hons). The member of the supervisory committee
is as follow:


DR. INTAN SHARHIDA BINTI OTHMAN
Pensyarah Kanan
Fakulti Kejuruteraan Pembuatan
Universiti Teknikal Malaysia Melaka

(Dr. Intan Sharhida Binti Othman)

ABSTRAK

Kajian ini menjalankan penyiasatan eksperimen terhadap pengaruh ketumpatan arus elektrodeposisi dan kehadiran natrium dodekil sulfat (SDS) ke atas sifat-sifat salutan komposit Ni-W-Debu kuari kitar semula. Objektif eksperimen ini adalah untuk mengkaji kesan pelbagai ketumpatan arus dan kandungan SDS ke atas morfologi, kekerasan, dan kehausan salutan komposit Ni-Debu Kuari Kitar Semula. Keluli lembut dipilih sebagai substrat kerana kerentanannya terhadap kehausan, kakisan, dan kekerasan yang rendah. Proses elektrodeposisi melibatkan penggunaan pelbagai ketumpatan arus untuk menganalisis kesannya ke atas hasil salutan komposit. Ketumpatan arus yang digunakan adalah antara 1, 3, 5, 7 hingga 9 A/dm², dan kehadiran SDS sebagai surfaktan berbeza pada kepekatan 0, 0.25, 0.50, 0.75, dan 1.0 g/L. Proses ini dijalankan dengan menggunakan elektrolit yang disambungkan kepada arus yang dibekalkan dan ketumpatan arus perlu dikawal. SDS akan ditambah ke dalam larutan dengan pelbagai kepekatan. Pencirian salutan dinilai menggunakan Mikroskop Elektron Imbasan (SEM) dan Pembelauan Sinar-X (XRD). Ujian Micro Vickers dan Pin on Disk akan menganalisis kekerasan dan kehausan substrat keluli lembut yang disalut. Hasilnya, peningkatan kandungan SDS mempunyai kesan yang ketara ke atas morfologi salutan pada ketumpatan arus yang lebih rendah, memihak kepada struktur yang lebih seragam dan padat. Ketumpatan arus yang lebih tinggi menyebabkan peningkatan kekasaran permukaan dan keliangan, yang mempengaruhi sifat mekanikal salutan. Selain itu, penggabungan debu kuari yang dikitar semula ke dalam salutan komposit menunjukkan peningkatan sifat-sifat tertentu yang menjanjikan. Ini menunjukkan kemungkinan kelestarian dan kos efektif dalam aplikasi salutan. Hasil ini menekankan betapa pentingnya parameter elektrodeposisi dan penggabungan aditif surfaktan dalam menyesuaikan ciri-ciri salutan komposit Ni-Debu Kuari Kitar Semula. Penemuan ini membuka jalan untuk mengoptimalkan penggunaan mereka dalam aplikasi industri, terutamanya dalam bidang perlindungan kakisan dan ketahanan kehausan.

ABSTRACT

This study conducted an experimental investigation into the influence of electrodeposition current density and the presence of sodium dodecyl sulphate (SDS) on the properties of nickel-recycled quarry dust (Ni-QD) composite coatings. The objective of this experiment is to investigate the effect of various current density and SDS content on the morphology, hardness and wear of the Ni-QD composite coatings. Mild steel was chosen as the substrate due to its susceptibility to wear, corrosion, and low hardness. The electrodeposition process was carried in nickel Watt's electrolyte at the temperature of 40°C and the current density in the range between 1 A/dm² to 9 A/dm². SDS which act as surfactant was added to the nickel Watt's electrolyte at 0, 0.25, 0.50, 0.75 and 1.0 g/L concentration. The coating was characterized by using scanning electron microscope (SEM) and X-ray diffraction (XRD). The hardness properties and wear behaviour of the coating were examine using micro-Vickers machine and pin on disc machine. As a result, an increase in SDS content (0.75 g/L) has a considerable effect on coating morphology at lower current densities (3 A/dm²), favouring a more uniform and compact structure. Higher current densities (9 A/dm²) applied cause to increase of the surface roughness and porosity, affecting the mechanical properties of the coatings. Furthermore, the incorporation of recovered quarry dust into composite coatings shows promise improvements in particular properties. Implying a possible sustainability and cost-effectiveness in coating applications. These results underscore the vital importance of electrodeposition current density and surfactant additives in customizing the characteristics and properties of Ni-QD composite coatings. This insight opens avenues for optimizing their utilization in industrial applications, particularly in areas such as corrosion protection and wear resistance.

DEDICATION

This research project is dedicated to:

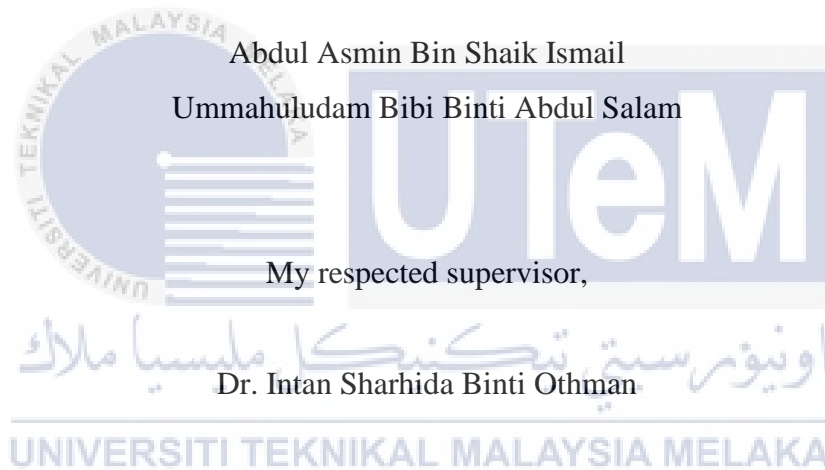
My lovely parents;

Abdul Asmin Bin Shaik Ismail

Ummahuludam Bibi Binti Abdul Salam

My respected supervisor,

Dr. Intan Sharhida Binti Othman



My siblings and friends,

I appreciate your moral support, financial assistance, encouragement, and understanding

Thank You So Much.

ACKNOWLEDGEMENT

In the name of ALLAH, the Most Gracious and Merciful,

I express my deepest gratitude to Allah for granting me the opportunity to successfully accomplish my final year assignment.

I extend my gratitude to my esteemed supervisor, Dr. Intan Sharhida Binti Othman, whose generosity, unwavering patience, and guidance supported me throughout the entire process. Her clear and accessible explanations, along with an open-minded approach, enabled my development and learning. I also want to express my heartfelt thanks to my dear family for their prayers and moral support, which proved instrumental in helping me overcome challenges during my study period.

In conclusion, I extend my heartfelt gratitude to my closest friends, whose unwavering motivation and mental support greatly contributed to the completion of this report. I would also like to express my appreciation to all technicians and others who, although not explicitly mentioned here, provided significant assistance in supporting the completion of this report. Special thanks are extended to the UTeM management, particularly the Faculty of Industrial and Manufacturing Technology and Engineering (FTKIP), for providing valuable opportunities that enhanced my knowledge and experience throughout the research period.

TABLE OF CONTENTS

ABSTRAK	i
ABSTRACT	ii
DEDICATION	iii
ACKNOWLEDGEMENT	iv
TABLE OF CONTENTS	v
LIST OF TABLES	ix
LIST OF FIGURES	x
LIST OF ABBREVIATIONS	xii
LIST OF SYMBOLS	xiv
CHAPTER 1	1
INTRODUCTION	1
1.1 BACKGROUND OF STUDY	1
1.2 PROBLEM STATEMENT.....	3
1.3 OBJECTIVES.....	4
1.4 SCOPE.....	4
CHAPTER 2	5
LITERATURE REVIEW	5
2.1 Composite Coatings.....	5
2.1.1 Types of Composite Coatings.....	6
2.1.2 Application of Composite Coatings	7
2.2 Electrodeposition of Nickel Coatings.....	9
2.2.1 The mechanism of nickel coating electrodeposition	9
2.2.2 Application of nickel coating electrodeposition	11

2.3	Parameter of Electrodeposition Process	12
2.3.1	Current density	13
2.3.2	Sodium Dodecyl Sulphate Surfactant (SDS).....	15
2.4	Steel Substrate	17
2.4.1	Types of Steel Substrate	18
2.4.2	Properties of Steel Substrate.....	19
2.5	Properties of Composite Coatings	21
2.5.1	Hardness	21
2.5.2	Wear resistance.....	23
2.5.3	Corrosion Resistance	25
CHAPTER 3.....		27
METHODOLOGY		27
3.1	Overview	27
3.2	Substrate preparation	29
3.2.1	Substrate cutting	29
3.2.2	Substrate Grinding and polishing	29
3.3	Quarry dust preparation	30
3.3.1	Quarry dust mill process.....	30
3.3.2	Quarry dust sieving process.....	31
3.4	Electrodeposition process	32
3.4.1	Nickel's watt bath.....	32
3.4.2	Electrodeposition Parameters	33
3.5	Material Characterization	34
3.5.1	Scanning Electron Microscope machine (SEM)	35
3.5.2	X-ray Diffraction machine (XRD)	35
3.5.3	Particle Size Analyzer	36
3.6	Sample Testing	36

3.6.1	Micro- hardness	36
3.6.2	Wear test.....	37
CHAPTER 4.....		39
RESULT & DISCUSSION		39
4.1	Characterization of Quarry Dust.....	39
4.1.1	Particle Size Analysis of Quarry Dust.....	39
4.1.2	Phase Analysis of Quarry Dust	41
4.1.3	Surface Morphology of Quarry Dust	41
4.1.4	X-Ray Fluorescence (XRF) of Quarry Dust	42
4.2	Characterization of Mild Steel Substrate	44
4.2.1	Energy Dispersive X-ray of Mild Steel Substrate.....	44
4.2.2	Surface Roughness of Mild Steel Substrate	45
4.3	Characterization of Nickel-Quarry Dust Composite Coatings	46
4.3.1	Visual Inspection of Nickel-Quarry Dust Composite Coatings.....	46
4.3.2	X-ray Diffraction of Nickel – Quarry Dust Composite Coatings	48
4.3.3	Surface Morphology of Nickel-Quarry dust composite coatings.....	51
4.3.4	Surface Roughness of Nickel-Quarry Dust Composite Coatings	53
4.4	Nickel-Quarry Dust Composite Coating Test.....	54
4.4.1	Hardness Test on The Nickel-Quarry Dust Composite Coatings	54
4.4.2	Wear Test on The Nickel-Quarry Dust Composite Coatings.....	56
4.4.2	Effect of Various Current Density and SDS Content on the Coefficient of Friction (COF).....	59
4.4.3	Energy Dispersive X-ray (EDX) on Wear Track	61
CHAPTER 5.....		64
CONCLUSION AND RECOMMENDATION.....		64
5.1	Conclusion	64
5.2	Recommendation	65

REFERENCES	66
APPENDICES.....	75
GANTT CHART PSM I.....	75
Gantt Chart PSM II.....	77



LIST OF TABLES

Table 3.1: Concentration of chemical in nickel's watt bath.....	32
Table 3.2: Electrodeposition operating condition table.....	33
Table 3.3: Experiment parameter table	34
Table 4.1: Element composition in quarry dust particles.....	43
Table 4.2: Element composition of mild steel substrate	45
Table 4.3: Experiment result.....	47



LIST OF FIGURES

Figure 2.1: Hardness value of Ni-Al Coatings on the SDS effects (Sabri et al., 2012a)	23
Figure 2.2: COF value of Ni-W-GO composite coatings (X. H. Zhang et al., 2019)	25
Figure 2.3: The polarization curve of Ni-W alloy with Ni-W-B4C composite coatings (He et al., 2018)	26
Figure 3.1: Flowchart of the experimental procedure	28
Figure 3.2: Dimension of the mild steel substrate	29
Figure 3.3: Grinding machine	30
Figure 3.4: Planetary ball mill machine, PM100	31
Figure 3.5: Octagon siever machine	31
Figure 3.6: The set up of electrodeposition process	32
Figure 3.7: Scanning Electron Microscope machine	35
Figure 3.8: X-ray Diffraction Machine (XRD)	36
Figure 3.9: Microvickers machine (Hardness-test)	37
Figure 3.10: Micro Pin on Disk Tribo Tester (CM-9109)	38
Figure 4.1: The particle size distribution of quarry dust (a) as received (b) after ball milling process for 5 hours at 350 rpm (c) after sieve using 63 μ m sieve pan.	40
Figure 4.2: XRD analysis of quarry dust particles	41
Figure 4.3: SEM observation of quarry dust particles (a) as received (b) After 5 hours of ball milling with 350 rpm	42
Figure 4.4: Pie chart of analyte concentration of quarry dust through XRF	44
Figure 4.5: EDX spectrum of mild steel substrate	45
Figure 4.6: Surface roughness of substrate	46
Figure 4.7: Solution overflow during electrodeposition process	48
Figure 4.8: The XRD result of nickel- quarry dust composite coatings (a) Without SDS surfactant and various current density and (b) 7 A/dm ² current density and various SDS content	50

Figure 4.9: Surface morphology of nickel-quarry dust composite coatings produce using 0.50 g/L SDS at various current density with (a) 1 A/dm ² (b) 5 A/dm ² and (c) 9 A/dm ² current density	52
Figure 4.10: Surface morphology of nickel-quarry dust composite coating produce at 5 A/dm ² of current density with various SDS content (a) 0 (b) 0.50 (c) 0.75 (d) 1.0 g/L	53
Figure 4.11: Surface roughness of nickel-quarry dust composite coatings	54
Figure 4.12: Hardness value of nickel-quarry dust composite coatings	55
Figure 4.13: Wear track of nickel-quarry dust composite coatings produce using 0.50 g/L SDS at various current density (a) 1 A/dm ² (b) 5 A/dm ² (c) 9 A/dm ²	57
Figure 4.14: Wear track of nickel-quarry dust composite coatings produce at 5 A/dm ² of current density with various SDS content at (a) 0 (b) 0.50 (c) 1.0 g/L	58
Figure 4.25: The COF value of at (a) various current density and 0.50 g/L of SDS content (b) various SDS content and 1 A/dm ² current density	60
Figure 4.16: EDX mapping on wear track of nickel-quarry dust composite coatings produce using 0.50 g/L SDS content with various current density (a) 1 A/dm ² (b) 5 A/dm ² (c) 9 A/dm ²	62
Figure 4.17: EDX mapping on wear track of nickel-quarry dust composite coating produce at 5 A/dm ² of current density with various SDS content (a) 0 (b) 0.50 (c) 1.0 g/L	63

LIST OF ABBREVIATIONS

AISI	-	American iron and steel institute
Al ₂ O ₃	-	Aluminium oxide
Al	-	Aluminium
AlTiN	-	Aluminium titanium nitride
AlCrN	-	Aluminium chromium nitride
AMC	-	Aluminium composite coating
ASTM	-	American society for testing and materials
B ₄ C	-	Boron carbide
C	-	Carbon
Cd	-	Cadmium
CER	-	Cavitation erosion resistance
CMC	-	Critical micelle concentration
CNT	-	Carbon nanotubes
COF	-	Coefficient of friction
Cr	-	Chromium
Cr ₂ O ₃	-	Chromium (III) oxide
CTAB	-	Cetyltrimethylammonium bromide
CVD	-	Chemical vapour deposition
DC	-	Direct current
EDC	-	Electrical discharge coating
GO	-	Graphene oxide
H ₂ SO ₄	-	Sulfuric acid
hBN	-	Hexagonal boron nitride
HCl	-	Hydrogen chloride
ISO	-	International organization of standardization
Mn	-	Manganese
Mo	-	Molybdenum

MoS ₂	-	Molybdenum disulfide
Na ₂ WO ₄	-	Sodium tungstate
Na ₃ C ₆ H ₅ O ₇	-	Sodium citrate
Ni	-	Nickel
Ni ₃ Ti	-	Nickel titanium
NiCl	-	Nickel (II) chloride
NiSO ₄	-	Nickel (II) sulphate
NiTi	-	Nitinol
Ni-W-B/B	-	Nickel-tungsten-boron/amorphous boron
NdFeB	-	Neodymium iron boron magnets
P	-	Phosphorus
PSA	-	Particle size analyser
PVD	-	Physical vapour deposition
QD	-	Quarry dust
QT	-	Quenching and tempering
S	-	Sulphur
SAE	-	Society of automotive engineers
SDS	-	Sodium dodecyl sulphate
SEM	-	Scanning electron microscope
Si	-	Silica
Si ₃ N ₄	-	Silicon nitride
SiC	-	Silicon carbide
SiO ₂	-	Sulphur dioxide
TiAlN	-	Titanium aluminium nitride
TiN	-	Titanium nitride
TiO ₂	-	Titanium dioxide
W	-	Tungsten
WC	-	Tungsten carbide
XRD	-	X-ray diffraction
2D	-	2-dimensional
3D	-	3-dimensional

LIST OF SYMBOLS

°C	-	Degree Celsius
μm	-	Micrometre
%	-	Percent
g/L	-	Grams per liter
wt. %	-	Weight percent
mm	-	Millimetre
nm	-	Nanometre
GPa	-	Giga Pascal
°C	-	Degree Celsius
rpm	-	Revolution per minute
A/dm ²	-	Ampere per square decimetre
mA/cm ²	-	Milliampere per square centimetre
mm/s	-	Millimetre per second
HV	-	Vickers hardness
L	-	Liter
min	-	Minutes

CHAPTER 1

INTRODUCTION

1.1 BACKGROUND OF STUDY

Mild steel is a ferrous metal composed of iron and carbon. It is a low-cost material with qualities appropriate for most common engineering applications. Low carbon mild steel has strong magnetic characteristics due to its high iron content and is thus classified as 'ferromagnetic'. Mild steel is widely utilised in the industrial and construction industries. The biggest issue with using mild steel in industry is its dissolving in acidic media solutions. Mild steel has little corrosion resistance, making it freely corroded. Mild steel is commonly used in industrial cleaning, oil field, petrochemical processing, heat exchangers, tanks, and other applications (Habeeb et al., 2018). To address this issue, epoxy coating has emerged as a widely adopted corrosion control method with diverse applications, including structural materials, tissue replacements, anti-corrosion coatings, and flame-retardant additives. In the field of material science, there has been significant interest in the amalgamation of organic polymers with inorganic particles, as noted by (Khodair et al., 2019).

In recent years, there has been an increase interest in research about composite coatings where it is known as subset of surface engineering. Composite coatings have been revolutionized through years across with the modern engineering application. As a basic definition, composite coatings consist of multiple materials where to achieve a unique and synergetic properties that are not present in any single component alone. These coatings are applied to the surface of substrate to enhance the mechanical properties, hardness, durability, and corrosion resistance (Lekka, 2018). Composite coatings, particularly those containing corrosion-resistant elements, act as a barrier against chemical and environmental degradation. Composite coatings also can improve mechanical strength and wear resistance of materials.

These coatings can endure abrasive forces by incorporating hard particles or fibres into a softer matrix, making them invaluable in industries such as industrial, automotive, and aerospace. The technique used to create a composite coating is normally by electrodeposition technique. Electrodeposition give several advantages like precisely controlled near room temperature operation, the capability to coat complex components geometries and simple scale-up for larger components.

Due to some environmental concern, composite coatings have a new pathway in transforming to sustainability and environmental responsibilities. The transformation is driven by several interrelated factors like resource scarcity, regulatory pressures, and consumer demands for eco-friendly. In this case, quarry dust is taken as an alternative material to combine with Ni to form a Ni -Recycled quarry dust composite coatings. Quarry dust is an alternative material that can be considered for use in composite coatings due to its environmental benefits. In addition to its positive environmental impact, quarry dust contains high amounts of Al_2O_3 and SiO_2 , which are valuable for composite coatings (Fadzli & Abdollah, 2019). By using quarry dust, the reliance on raw Al_2O_3 and SiO_2 can be reduced, as it serves as a recycled material. The hardness and strength properties of quarry dust add extra value to the coating materials. This not only decreases the need for purchasing raw materials but also promotes the use of recycled materials.

A key aspect of composite coatings is the electrodeposition technique. Electrodeposition techniques provide various advantages such as precise temperature control, the ability to cover complicated components, and cheap cost. Several studies have found that the tendency of produce composite coatings via electrodeposition technique getting rise due to its superior properties. In summary, electrodeposition involves the transfer of electrons to ions in a solution, resulting in the deposition of a thin layer of one metal onto another, thereby altering its surface properties (Shen et al., 2019). The coating layer appear on the metal plate plays a crucial role as a guard to keep the surface properties from any harm. The coating also gives some added value on the metal plate upon the finishing process. The main factors that help in the electrodeposition technique is the number of current densities applied. Current density of the electrodeposition process is the main parameters that need to be controlled to get a best result of coating process. The electrodeposition process also helps a lot in the coating process especially to coat some complex coatings. By applying a proper amount of current density, it can help to coat some complex coatings. To achieve a good coating outcome,

difficulties such as uniformity of coating, porosity and flaws, and energy consumption must be addressed in a series of steps.

To form a good composite coating, it needs some addition of surfactants. Surfactants play as a chemical compound that significantly influence the behaviour of solids and liquids at interfaces. These adaptable molecules have a one-of-a-kind structure, with one end hydrophilic (attracted to water) and the other end hydrophobic (repelled by water). Surfactants play an important role in coating processes, delivering multiple advantageous qualities to the coatings, and changing their behaviour in a variety of ways (Zolfaghari et al., 2019). In this coating process, surfactants that are used are sodium dodecyl sulphate (SDS). Sodium dodecyl sulphate (SDS) is important where it disperses quarry dust in the composite coatings process. SDS also helps in the prevention of particle agglomeration or clumping in the coating solution. Presence of SDS will ensure that the quarry dust will be dispersed uniformly throughout the composite coatings, improving mechanical characteristics and overall uniformity.



1.2 PROBLEM STATEMENT

Raw materials used in industrial applications frequently experience failures due to wear, corrosion, and hardness issues. Mild steel, commonly used in the automotive and construction sectors for its machinability and weldability, faces similar challenges. To address these problems, surface treatments are necessary to enhance mild steel's properties.

Electrodeposition is an effective, economical surface treatment method that can improve mild steel's resistance to wear, hardness, and corrosion. The effectiveness of this process is influenced by its parameters, particularly current density, which is crucial for achieving a well-distributed inert particle coating on the surface. Proper current density is essential for uniform Ni coating distribution during electrodeposition. Combining nickel and tungsten to form a matrix composite, this method aims to coat mild steel and improve its properties.

Additionally, incorporating quarry dust, a byproduct of quarrying activities, as a reinforcement in the composite coating can further enhance mild steel's properties. To ensure uniform distribution of reinforcement particles, a surfactant such as SDS will be added to

the solution. Varying the SDS surfactant content will help determine the optimal amount needed to affect the morphology of composite coatings.

However, the precise effect of SDS on the properties of nickel-recycled quarry dust composite coatings remains unclear. Therefore, the aim of this research is to investigate how electrodeposition current density and SDS surfactant content influence the characteristics of nickel-recycled quarry dust composite coatings.

1.3 OBJECTIVES

- (a) To investigate the influence of various current density on the morphology, hardness properties, wear behaviour of Ni-Recycled quarry dust composite coatings.
- (b) To study the effect of sodium dodecyl sulphate content on the morphology, hardness properties, wear behaviour on the surface of the Ni-Recycled quarry dust composite coatings.

1.4 SCOPE

The composite coating layer consist of combination of nickel-tungsten and quarry dust. This combination of composite coatings is done by using electrodeposition method with varieties of current densities like 1,3,5,7 & 9 A/dm². Electrodeposition method is using electrolyte that connected to a direct current source where it is done in glass cell. The substrate represents the mild steel or low carbon steel and the anode represented by nickel. The electrolyte solution consists of NiSO₄, NiCl₂ and Na₃C₆H₅O₇. Addition of sodium dodecyl sulphate surfactant (SDS) in the solution to help in the disperse of quarry dust to the substrate. The quarry dust disperse is help by the stir bar where it will stir the solution to help sodium dodecyl sulphate in dispersing the quarry dust to the substrate. SEM, XRD, mickro-vickers and Pin on disc are some of the equipment that will be analysed the microhardness, corrosion resistance, physical properties, and wear and friction coefficient of substrate.

CHAPTER 2

LITERATURE REVIEW

2.1 Composite Coatings

A composite coating is a mixture of protective layers applied to a substrate like steel and concrete. Composite coatings prevent substrate corrosion by incorporating at least two ingredients. These compounds are often composed of two or more layers of epoxy resin and polyurethane synthetic resin. According to (Lekka, 2018), Composite coatings are a low-cost approach of improving the resistance of metallic components to adverse operating conditions and increasing component service life by improving mechanical, thermomechanical, tribological, and corrosion properties. When contrasted with a basic metal or alloy matrix system, it can be demonstrated that these materials display enhanced mechanical, electrochemical, lubricating, and high-temperature properties. Consequently, composite coatings are frequently employed to extend the operational lifespan of mechanical components, cutting equipment, and electronic parts subjected to challenging conditions (P. Zhang et al., 2023)

2.1.1 Types of Composite Coatings

a) Metal Matrix Composite Coatings

According to (Das & Das, 2021) Metal matrix composites (MMCs) are materials where fibers or particles are embedded within a metal matrix. These composites exhibit exceptional stiffness and strength, along with superior temperature resistance compared to polymer matrix composites (PMCs) and pure metals. Additionally, MMCs offer advantages such as improved abrasion and creep resistance, resistance to fluid degradation, dimensional stability, and non-flammability. Despite these benefits, their practical applications are restricted due to the higher weight and cost associated with their production. Another study by (Isern et al., 2024) state that metal matrix composite (MMC) coatings consist of two distinct phases: a continuous metallic phase serving as the matrix and a dispersed phase comprising particles, which can range from ceramics to metals and polymers. Various methods have been successfully employed to deposit MMC coatings, including thermal spraying, plasma spraying, high-velocity oxy-fuel spraying, chemical vapor deposition, laser cladding, and electroplating.

b) Polymer Matrix Composite Coatings

Polymer matrix composite is explained well by (Rajak et al., 2019) where they state that Polymer matrix composites (PMCs) consist of a thermosetting or thermoplastic matrix reinforced with materials such as carbon, glass, Kevlar, or metal fibers. Thermosetting plastics are more commonly used than thermoplastics due to their superior strength and high-temperature resistance. They are produced by mixing resin with a hardener. The most prevalent form of PMCs is the laminar structure, created by stacking and bonding thin layers of fiber and polymer until the desired thickness is achieved. PMCs are considered low-cost composites because of their straightforward handling and fabrication processes. Another source from (Wu et al., 2023) states that polymer composite materials are primarily composed of high-performance fibers (such as carbon fiber, glass fiber, and aramid fiber) as reinforcement and matrix materials (such as epoxy resin). The matrices of polymer composites are typically categorized into thermoplastic and thermosetting types, both of which are extensively utilized in aerospace, aviation, biomedicine, automotive parts, electrodes, and packaging materials.

c) Ceramics Matrix Composite Coatings

According to (Sun et al., 2023) ceramic matrix composites (CMCs) are composed of one or more types of reinforcement such as fibers, whiskers, carbon nanotubes (CNTs), graphene, particulates, and second polymers or metal phases embedded within a ceramic matrix. These composites generally offer superior strength and wear resistance, excellent fracture toughness, high-temperature stability, and outstanding thermal shock resistance. The exceptional mechanical and physical properties of CMCs make them highly desirable for applications in aerospace and defense, automotive, energy and power, electronics and electrical, and chemical and biomedical engineering industries. These diverse applications are driving the demand in the ceramic matrix composites market. Based on (Shrivastava et al., 2024) they stated that ceramic matrix composites (CMCs) are represent a significant advancement in materials science and engineering, as they combine the remarkable properties of ceramics with the strength and toughness of fibers. Their unique qualities offer enhanced performance and durability in harsh environments, garnering substantial interest across various industries. As a subgroup of both composites and ceramics in materials research, CMCs consist of fibers or particles embedded in a ceramic matrix. They are renowned for their ability to withstand extremely high temperatures and corrosion, as well as for their lightweight nature and robust chemical stability, which prevents reactions with other chemicals or materials. These attributes make CMCs ideal for applications with stringent mechanical and thermal requirements.

2.1.2 Application of Composite Coatings

Wide range of the composite coatings are being applied like corrosion control on steel, bridges, offshore platforms, underground pipelines, and other structures. It is often made up of many chemicals such as thermoset polyimide, fluoropolymer composite paints, and polyamide binders (Corrosionpedia, 2019). In this study, the application is focused directly on Ni-W-Recycled quarry dust composite coatings. A study done by Allahyarzadeh et al., (2016) found that the nickel-tungsten alloys are mostly employed as hard and wear-resistant coatings due to its great hardness and wear resistance. Furthermore, the adequate corrosion resistance of these alloys has enabled its application as hard coatings with significant corrosion resistance. Furthermore, it has been observed that Ni-W films have

favourable electrocatalytic characteristics. As a result, Ni-W, Ni-Mo, and Ni-W-Mo alloy systems are recognised as suitable catalysts for the hydrosulfuration and hydrogenation of diverse organic molecules and petroleum products. Another source from Li et al., (2017) state their opinion that Ni-W alloys are well-known for their advantageous qualities such as high mechanical performance, resistance to corrosion and magnetism. These unique properties have made it suitable for broad use as a metallic matrix, and numerous particles, including TiO₂, Al₂O₃, SiO₂, WC, SiC, diamond, CNT, Cr₂O₃, MoS₂, and Si₃N₄, have been electrochemically integrated into Ni-W alloys. Besides Ni-W based coatings, the addition of recycled quarry dust will improve the mechanical properties of the coating surface. Based on the study done by Yap et al., (2020) they agreed that without the quarry dust addition, the coated surface developed micropores and microcracks, resulting in a poor surface quality. Besides, the EDC process done by them effectively deposited quarry dust components such as Si, Fe, Ca, Al, Mg, and Zn on the WC-Co substrate, and the coating layer thickness rose considerably with quarry dust concentration. So, the presents of quarry dust in the matrix coating might influence the mechanical properties of the composite coating on the substrate surface.

A study done by Tan et al., (2023) found that, materials are subjected to high temperatures in a variety of applications, including engines and aircraft. Coating and base materials that can withstand high temperatures have important hurdles in terms of oxidation resistance, microstructural and mechanical capabilities in the design. Ni is resistant to oxidation up to 500 C, hence Ni-based alloys or co-depositions are feasible at higher temperatures. Ni-W coatings are more resistant to oxidation than other nickel-based coatings due to tungsten's diffusion barrier characteristics at high temperatures. Ni-W coatings may be suitable for high temperature applications due to their superior mechanical properties, resistance to oxidation, and high melting point. That is an example of application in aerospace and automotive industry that used Ni-W based coatings to protect the surface from corrosion because of its good performance in mechanical properties. Despite, research done by Alaneme & Bamike, (2018) demonstrate that the use of quarry dust as composite coatings is successful in aluminium composite coatings (AMCs) because of its successful usage and commercialization in a few applications including automotive, aircraft, marine, defence, and thermal management. Quarry dust, a byproduct of rock/stone crushing, is recommended in this study as a replacement for SiC with the goal of filling gaps observed in agricultural and industrial wastes previously used as reinforcement in AMCs. So, the combination of Ni-W-

recycled quarry dust could give much more benefits in terms of hardness to the applied surface.

2.2 Electrodeposition of Nickel Coatings

Kannan et al., (2019) define electrodeposition as a non-vacuum electrochemical process that is widely preferred for thin film deposition due to its ability to form multicomponent alloys at low temperatures. Thin metallic films are deposited onto the substrate using this approach without any undesired reactions. In Zhang et al., (2020) research, they feel that composite electrodeposition of nickel with nanoparticles or microfibers, which are considered as the second phase incorporated into the nickel matrix, is a potential strategy for reaching their study aims. It is because they want a type of surface coating that high in wear resistance and low coefficient friction where they believe that electrodeposition of nickel and nanoparticles can give a promising impact. In Walsh et al., (2020) findings, electrodeposited composite coatings provide customised corrosion protection, electronic conduction, corrosion, and wear resistance have resulted in a wide range of industrial markets such as aerospace, textile, automotive engineering, and general engineering. So, the characteristic that bring by the effect of composite coating electrodeposition is useful in real life applications.

2.2.1 The mechanism of nickel coating electrodeposition

Due to its speciality as low-cost, and low temperature technique, electrodeposition techniques are the most effective methods that been applied in the industry nowadays. A finding by Bigos et al., (2021) states that many investigations have been conducted on the electrodeposition of nickel coatings from aqueous solutions. Baths of many sorts, including sulphamate, acetate, chloride, sulphate, lactate, and propionate and gluconate salts, can be utilised in the operation. In Lelevic & Walsh, (2019) research on Ni-P electrodeposition, they investigated and propose that Ni-P coatings, with careful composition and structural tailoring, might give adaptive solutions to a wide range of environmental and operational

situations. Unlike chromium coatings produced in hexavalent chromium baths, the effluents from nickel electroplating can be treated with less complexity, for example, utilizing Clean Technologies such as electrodialysis. Depending on the electroplating variables and the post-treatment, Ni-P coatings exhibit a range of fascinating features. Deposits are frequently distinguished by superior mechanical qualities, strong wear- and corrosion resistance, electrocatalytic activity, and advantageous tribological properties.

According to Wu et al., (2021), the predominant method in electroplating and industrial sectors for Ni electrodeposition involves the use of watts electrolyte. The watts bath offers various advantages, including high current density, efficient heat dissipation, rapid formulation, and a wide operating pH range from 2.0 to 5.0. The nucleation process for Ni electrodeposit from watts electrolyte encompasses both 2D (layer growth) and 3D (nucleation-coalescence growth) crystallite growth. In the former, crystal formation occurs by sequentially spreading individual layers over the surface. In the latter approach, an isolated nucleus develops into a 3D crystallite, which then combines with numerous other 3D crystallites to form a continuous deposit. The growth mode of the deposits can significantly influence the growth and textural development of Ni coatings. According to Shen et al., (2019) on their research of superhydrophobic nickel coating, they found out that the influence of electrodeposition on the surface morphology. In their findings, they stated that during the initial stages of electrodeposition, a relatively flat cathode surface facilitated nickel ion reduction and nucleation, leading to the continuous growth of crystal nuclei. The growth was irregular due to surface imperfections, causing varied growth rates across the substrate. Consequently, fast-growing regions formed protrusions, creating uneven surfaces with increased current density and faster deposition rates. These protrusions evolved into dendritic structures, inhibiting growth in surrounding areas and resulting in the formation of cauliflower-like clusters. According to a study by Priyadarshi, Piyush, Kishore, Kamal, and Maurya, Rita., (2022), the thickness of Ni coatings produced by the electrodeposition technique changes linearly with time. The simulation showed a maximum thickness of 32 μm after 3600 seconds, equivalent to an hour. As a result, the electrodeposition process is important in the creation of surface morphology. The pattern of formatted surface morphology may also be affected by current density.

2.2.2 Application of nickel coating electrodeposition

The electrodeposition process of nickel coatings is being applied in various industries. A review conducted by Karimzadeh et al., (2019) on electrodeposited Ni-Co alloy and composite coatings revealed that electrodeposition is a widely adopted method for producing Ni-Co coatings. This popularity stems from its cost-effectiveness, flexibility (enabling single or multilayer deposition in intermittent or gradient patterns), high efficiency, and straightforward mass production procedure. Notably, electrodeposition imposes fewer requirements in terms of increased temperature and pressure compared to alternative manufacturing methods like chemical vapor deposition (CVD), sputtering, and flame spraying. The advantages inherent in the electrodeposition process make it applicable across various industries. Meanwhile, Zhang et al., (2020) also agreed that Electrodeposition is a relatively easy and cheap procedure that is frequently used in the creation of nanomaterials, hydrophobic surfaces, and composite coatings. They assume that when it been deposited on metal surface, the metal substrate would be protected by nickel from corrosion. When the nickel combined with hydrophobicity, it has a significant potential for use as corrosion and contaminant resistant materials.

In terms of corrosion resistance applications Yang et al., (2019) they note that Nickel is an important industrial material. due to its exceptional corrosion resistance, hardness, and magnetism in their research on the electrodeposition creates a super-hydrophobic nickel coating on a copper substrate to boost corrosion resistance. When nickel is added to a copper substrate, it prevents corrosion of the bare copper. Because of its high hydrophobicity, the deposited nickel coating can offer distinct advantages such as self-cleaning and corrosion resistance. According to Anwar et al., (2019) they give various advantages of nickel matrix coating via electrodeposition. In their research, they are trying to find alternative material that can exchange with cadmium (cd) due to environmental issues. They are focused to reduce corrosion on marine and offshore structures. As an alternative they are trying to form Zn-Ni coating due to advantages of nickel alloy that good in corrosion resistance properties. In their research also, they found that this nickel alloy is widely used in automobile industries as a matrix composite. Zn-Ni alloy may have better thermal and mechanical qualities than pure Zn and other Zn alloys. The electrodeposition of the Zn-Ni alloy enhances the corrosion resistance of coated steel structures in hard environments significantly. Currently, Zn-Ni

alloy coatings offer an essential environmentally favourable alternative to toxic cadmium coatings.

In mechanical and wear resistance aspects Wasekar et al., (2020) state that the electrodeposition of nickel based composite coatings give a superior property compared to other coating method like flame spraying, nitriding, and hard chrome plating where it applied in aerospace, marine, mining and electrical. They also added that based on their research, to enhance the wear and corrosion resistance of Ni-W coating, it can consider adding another material to improve the properties. It can be Ni-W-Si composite coatings or others element that suitable can bring advantages in term of wear and corrosion resistance. Sajjadnejad et al., (2021) also agreed that electrodeposition provides an exact control of manufacturing conditions, resulting in variable coating qualities, and it can coat components with complicated geometry. They also added that the coating fabrication may be done at a low cost, atmospheric pressure, low temperature, and with simple to use and reduce maintenance equipment, making electrodepositions a viable option for industrial applications. In the process of electrodeposition for composite coatings, suspended insoluble particles within the plating solution, typically held by electrostatic repulsion, become entrapped within the developing metal film. Such particles commonly enhance the wear resistance characteristics of the composite coatings to a notable extent. So, the electrodeposition process helps much in the nickel coating process. It plays a significant role where it influences might change the surface morphology, characteristics and tribological properties of the coating surface. The electrodeposition also highlighted some mechanical elements like wear and corrosion resistance where it improves the mechanical and wear properties of the coated surface. So, with all this advantages in electrodeposition and low cost it is not surprise why industries are choosing electrodeposition process rather than other deposition process.

2.3 Parameter of Electrodeposition Process

According to Mersagh Dezfuli & Sabzi, (2019) on their research that highlighted, electroplating is a procedure that may be used to create a nanoscale structure if the plating conditions such as bath composition, temperature, pH, potential difference, and other variables contribute to high nucleation and decreased grain development. They also state

that the formation of grain growth and nucleation of new crystal are influenced by the electrodeposition parameter. The formation of growth grains occurs when high surface diffusion rate and low potential differences while at low surface diffusion rate and high potential differences the nucleation of crystal are formed. Alizadeh & Cheshmpish, (2019) on their findings state that, based on their research most researchers are used electrodeposition process because of its parameters like electrolyte pH, electrolyte composition, reinforcement concentration and current densities. Current densities serve as a crucial factor in influencing the chemical composition, microstructure, mechanical, and corrosion properties of the deposited coatings across various parameters. Therefore, the composite coatings' parameters play a pivotal role in shaping the characteristics of the deposited coatings. The determination of all electrodeposition parameters is essential to enhance the quality of the coating.

2.3.1 Current density

Current density is one of the electrodeposition parameters where it might influence the surface morphology and properties of the coated materials. Based on Li et al., (2019) research, they found that many researchers agree that current density seriously give impact to the hardness and corrosion resistance. On their first findings, the researcher fabricates Ni/GO coating with current density of 2-6 A/dm² and it resulted to its hardness and corrosion resistance. The next researcher produces the asplated Ni-P-TiO₂ nanocomposite with 15 A/dm² current density have been applied and it enhance the hardness and corrosion resistance due to high content if Ni₃Ti. Another researcher fabricates Ni-Co/SiC nanocomposite current density affects the microstructure and high amount of current density is an important factor in determining the grain size. Based on Oliveira et al., (2021) they state that the intensity of the electromotive force of ionic attraction up to the cathodic surface is related to the current density. It is proved by their experimental on the properties of Ni-W-Co by electrodeposition where the current density has a good influence on the alloy composition when it was reviewed in the extrapolated factorial design. The deposition of Ni occurs when current density increased to 120.45 mA/cm² while the deposition of Co-occurs when current density at the range of 19.55 mA/cm². Based on their result, they agreed on

their findings that state the increasing amount of current density might affect the reaction of Co on the nucleation rate and increase the Ni content that might change the three-dimensional structure of the coating where it helps in increasing the surface area.

According to Yamamoto et al., (2019) on their research about the influence of current density on the mechanical properties of electroplated nickel, they are focusing on the surface morphology and mechanical properties. They state that, the growth rate in the electroplating is highly related to the current density where the rate growth will increase along with the high rate of current density. Results from their experiment on the surface morphology shows that a conical shape structure appeared on the electroplated when $10\text{mA}/\text{cm}^2$ of current density are applied. When the rate of current density is increased to $20\text{mA}/\text{cm}^2$, the conical shape structure starts to disappear and form a smooth and dense surface. The current density rate is rise again to $100\text{mA}/\text{cm}^2$ and it resulted to no pinhole or defects occurred on the nickel plate. The examination of grain sizes revealed a significant impact of the current density rate. As the current density increased from $10\text{ mA}/\text{cm}^2$ to $20\text{ mA}/\text{cm}^2$, a reduction in grain size was observed, decreasing from 2549.6 nm to 349.8 nm . The grain size is contingent on the cathodic overpotential, closely linked to the current density according to the Butler-Volmer equation. Beyond a current density of $20\text{ mA}/\text{cm}^2$, there was an increase in grain size, potentially allowing for a side reaction leading to the formation of hydrogen. In nickel electroplating, the hydrogen evolution is an unavoidable side reaction, and the hydrogen evolution might higher than nickel reduction when current density is high. On the hardness result, the hardness increases when the current density is increase from $10\text{mA}/\text{cm}^2$ to $20\text{mA}/\text{cm}^2$. When the current density exceeds $20\text{mA}/\text{cm}^2$, the hardness started to reduce, and the highest rate of hardness test were observed at $20\text{mA}/\text{cm}^2$. Based on Hall-Petch relationship, the hardness is inversely proportional to grain size. It is mean that the hardness is increase when the grain size is small. Kollé et al., (2020) state that on its research that at low current densities, the morphology of the Ni-W coating was smooth and homogeneous, but as current density increased, the structure became needle-shaped. Likewise, the applied current density plays a significant role in shaping the mechanical properties and composition of the coatings. According to their experimental findings from the microhardness test, an increase in the applied current density results in a corresponding rise in microhardness. The peak microhardness values were recorded at 920 HV when the applied current density was $60\text{ mA}/\text{cm}^2$. This effect is attributed to the incorporation of higher tungsten (W) content at elevated current density, leading to the formation of a solid solution. The observed increase

in microhardness readings with rising current density may be attributed to a reduction in crystallite size and/or an increase in lattice stresses. Therefore, the impact of current density extends to the surface morphology, hardness, wear resistance, and corrosion resistance of the substrate.

2.3.2 Sodium Dodecyl Sulphate Surfactant (SDS)

Mousavi et al., (2019) emphasize the significance of agents in electroplating for achieving lustrous deposits. In the electrolysis process, surfactants, serving as surface-active additives, are pivotal in influencing distinct characteristics of the electrodeposited layer, including its brightness. Based on their discoveries, the morphology of the C0S1 coating sample resulted from an electroplating bath solution with solely 0.1 g/l SDS as an anionic surfactant. A comparison indicates that the deposition conditions are more advantageous when SDS is used as an anionic surfactant in contrast to CTAB as a cationic surfactant. Nevertheless, despite the inclusion of 0.1 g/l SDS, a thorough examination reveals the existence of supplementary pores in the coating, implying a pronounced hydrogen evolution under these circumstances. Cathodic polarization curves acquired from a solution with 0.1 g/l anionic surfactant demonstrate a shift toward positive potentials upon the introduction of 0.1 g/l SDS, mirroring the effect observed with the cationic surfactant. This shift reduces hydrogen evolution overvoltage. The coating, however, exhibits numerous holes, indicating rapid hydrogen evolution. The presence of pores is suggested as the main reason for the decrease in Mo content from 8.5 to 4 Wt.% in the coating, as most of the cathodic current is consumed by hydrogen evolution, leading to a decreased alloy deposition rate. With the elevation of SDS concentration to 0.5 g/l in the electroplating bath, there is an observable shift of the cathodic polarization curve towards negative potentials, indicating the mitigation of hydrogen evolution due to heightened overvoltage. This augmented polarization leads to a decline in the concentration of metallic ions at the interface of the electrolyte and cathode. The C0S5 coating sample shows a reduction in Mo content to 3.7 Wt.% when the SDS concentration is raised to 0.5 g/l, validating the existence of concentration polarization under these circumstances.

In their study, Zolfaghari et al., (2019) emphasized the significance of surfactants in augmenting the repulsion force among particles possessing like charges. This mechanism prevents agglomeration and results in a solution containing more stable particles. Surfactants were frequently employed in electrodeposition baths to generate coatings with varied characteristics. This was illustrated in their research, where the researchers extensively investigated the impact of surfactants on surface morphology and roughness. As per their experimental findings, the arrangement of Ni particles in electrodeposited samples is governed by the dispersion of particles within the solution. When particles approach each other, their behaviour is influenced by either attraction or repulsion, determined by the energy between them. Owing to stronger attraction forces, particles tend to agglomerate. Nevertheless, when SDS is employed as an anionic surfactant, it gets adsorbed onto the nanoparticle surfaces. This causes nanoparticles with analogous charges to repel each other, resulting in a more even dispersion. In samples where SDS concentration equals the critical micelle concentration (CMC), the distribution of nanoparticles is uniform. Conversely, when SDS concentration is higher or lower than the CMC, Ni particles aggregate, indicating particle congregation. The PRC technique, characterized by the reversal of current direction, triggers consecutive adsorption and desorption events of SDS on the material's surface. This process gives rise to a porous nanocrystalline structure with certain agglomerates. The application of this method enhances the comprehensive comprehension of how surfactants impact particle distribution and morphology in electrodeposited coatings.

In their study, Yasin et al., (2018) underscored the influence of two distinct surfactants, namely cetyltrimethylammonium bromide (CTAB) and sodium dodecyl sulphate (SDS), on the characteristics of coated materials. Their experiments specifically utilized SDS as a surfactant, impacting the surface morphology and carbon content of nanocomposite coatings. The investigation delved into the varying effects of SDS concentrations on the surface morphologies of nanocomposite coatings formed in a deposition bath containing 0.2 g/L graphene. The study elucidated the impact of the anionic surfactant SDS on surface morphologies, comparing composite coatings produced from electrolytes with and without SDS. The introduction of SDS notably augmented the roughness of the composite coatings. An increased concentration of SDS in the fundamental bath solution, especially at 0.4 g/L, resulted in a significant elevation in the roughness of the coatings. The heightened SDS content in the deposition bath gave rise to a distinct bulge morphology, incorporating graphene nanosheets and nickel within the coatings. Throughout

the electrodeposition process, nickel ions migrated and were deposited on the cathode surface, with graphene sheets tending to amalgamate into a newly formed nickel matrix. The agglomeration of graphene nanosheets, exacerbated by their high conductivity and small size, contributed to the development of bulges. The accelerated deposition of nickel ions surrounding graphene sheets played a role in the increased bulging morphology of the composite coatings. Moreover, an elevated SDS concentration facilitated improved dispersion of graphene sheets in the electrolyte, fostering enhanced co-deposition through electrostatic repulsion among the graphene sheets, preventing aggregation and ensuring a rapid and uniform deposition. The presence of SDS in the electrolyte also led to the adsorption of negative functional groups on the graphene sheets, thereby increasing nickel ion deposition around them. Therefore, the SDS content played a crucial role in influencing the properties and surface morphology of the coated substrate. Understanding the functionality and characteristics of SDS is essential to ensure the proper addition of SDS to the nickel's watt bath solution, preventing any unwanted agglomeration on the substrate.

2.4 Steel Substrate

Steel is widely used in a variety of sectors, including the construction of bridges and large structures. Steel is used extensively in the manufacture of maritime furnishings and offshore platforms. Steel used in construction frequently necessitates the use of fire-defence measures to reduce the enormous cost of fire in terms of asset loss and life hazard (Puspitasari et al., 2019). Li et al., (2018) state that mild steel is widely used in the building and manufacturing industries, but corrosion has become a global concern with significant economic costs and, in some cases, disastrous effects when rust causes steel structures to collapse. According to Hoche et al., (2020) coating is important to corrosion-prone steel substrates, such as unalloyed and low-alloyed quenching and tempering steels. As a result, corrosion-resistant (and hence expensive) substrates must be employed, greatly reducing their economic efficiency in comparison to typical low-alloy quenching and tempering (QT) steels.

2.4.1 Types of Steel Substrate

Fotovvati et al., (2019) highlight several challenges faced by substrates that necessitate treatment to improve their properties. For instance, NiTi alloys are renowned for their shape memory effect (SME) and superelasticity (SE), offering opportunities for creating new actuators. Additionally, these alloys, when utilized as bone implants, exhibit high biocompatibility, and can be combined with SME, SE, or both to develop innovative biomedical devices for micro-surgeries within the human body. However, in physiological conditions, the corrosion of NiTi generates Ni ions as byproducts, which are toxic and hazardous compounds for living organs. In contrast, copper, known for its excellent thermal and electrical conductivity with various applications, such as brazing advanced materials, possesses low stiffness and wear resistance. The susceptibility of copper to wear mechanisms significantly reduces the durability of mechanical components, especially in the case of copper rotating cooling fins. To address these challenges and enhance their mechanical properties, the authors suggest subjecting these materials to a coating process, which proves to be a cost-effective solution. As indicated by Szala et al., (2019), stainless steel grade AISI 304 (SS) stands out as one of the extensively utilized contemporary structural materials. This preference is attributed to its exceptional corrosion resistance, favourable mechanical characteristics, acceptable weldability, and good formability. However, its resistance to sliding wear and cavitation erosion (CER) is somewhat limited. To address this limitation, the wear resistance of stainless steel can be improved through the application of various hard coating systems. Examples include TiN, AlTiN, TiAlN, or AlCrN. Alternatively, enhancement can be achieved by depositing stainless steel coatings that are further coated with silver.

In Natarajan et al., (2021) research, their focus is on 316L stainless steel, which serves both as a coating and substrate. This stainless-steel grade, containing higher percentages of chromium (18%) and nickel (10%) along with other elements such as C, Mn, Si, S, P, exhibits corrosion and oxidation resistance. It finds optimal application in high-temperature environments, including boiler tubes, heavy water plants, and heat exchangers. However, prolonged exposure of 316L steel in such harsh conditions leads to material

property degradation, ultimately resulting in component failure. The research emphasizes that 316L steel components in the oil and gas sector are prone to sliding and erosion wear due to chemical reactions with the surface. In environments containing chlorides, sulphides, or fluorides, the susceptibility of 316L steel to corrosive assaults at high temperatures is highlighted. The formation of corrosive acids like HCl and H₂SO₄, resulting from the reaction with precipitates, contributes to the corrosion of 316L steel. Additionally, stress corrosion fractures have been identified in 316L steel tubes within high-pressure water reactors, attributed to the impacts of water softening agents, causing caustic corrosion on tube walls. Therefore, under hostile conditions involving high temperature, high pressure, and the presence of corrosive salts, corrosion in 316L steel components is triggered. In another research by Kul et al., (2020) they report that Steel is the most extensively utilised material in a variety of industrial applications due to its superior mechanical qualities. Steel, on the other hand, has a low resistance to corrosion, which is sometimes addressed by covering its surface with a protective layer. To enhance its corrosion resistance, they applied electrodeposition process to coat the steel. As cathodes, SAE 1010 steel substrates with dimensions of 20x100x1 mm were employed. So, the SAE 1010 are the type of steel that examined by them to improve its corrosion resistance properties. As a result, while all pure and raw steel materials have different qualities, they still require some treatment to improve their attributes for the greater benefit of their use. It is determined by the steel's status and qualities whether to proceed with heat treatment, electrodeposition, vapour deposition, or other surface treatments.

2.4.2 Properties of Steel Substrate

Steel substrates are frequently treated to improve their characteristics. The qualities of the steel substrate will be determined to determine if it is suitable for use in certain applications. In Parhizkar et al., (2018) research, they stated that organic coatings considerably increase the corrosion resistance of steel substrates by acting as a passive barrier between the steel substrate and the corrosive environment. They are trying to improve the steel substrate properties in terms of corrosion resistance. Singh et al., (2020) state that Surface engineering is the most common approach for increasing a material's surface qualities and functioning without changing its bulk properties. This approach is useful for

changing a material's surface to produce surface characteristics that differ dramatically from the material's bulk properties. Corrosion protection for ferrous alloys (mild steel, stainless steel) used in the oil and gas sector is an important area of study. In material engineering applications, mild steel is the commonly used material, but it has very poor corrosion resistance. Various applications can be applied to enhance its properties like PVD, heat treatment, thermal spraying, and electrodeposition.

According to Sunday Isaac Fayomi & Patricia Idowu Popoola, (2019) findings, they state that mild steel the most common and one of the world's most affordable and useful metals. It is primarily iron and carbon alloys with minor additions of metals such as manganese and silicon to provide the necessary mechanical characteristics. The characteristics of mild steel are mostly determined by the quantity of carbon present. Mild steel includes up to 0.25% carbon as a component, among other things. This enabled it to be used in a variety of items, including structural beams, automotive bodywork, kitchen appliances, and cans treatment. They also agreed that mild steel is chosen for attributes other than corrosion resistance, such as strength, simplicity of fabrication, and cost. Mild steel is mostly resistant to alkalis, many organics, and strong oxidising acids. In different source from Suleiman et al., (2020) they explained that mild steel (MS) is an important component of the infrastructure of many sectors, including the oil and gas industry. However, corrosion-induced degradation of this material produces more substantial deterioration concerns in steel structures in these sectors. So, they come out with one solution where the mild steel need coat to enhance its mechanical, corrosion and wear properties. Various method can be used to coat the mild steel like PVD, thermal spraying and electrodeposition process. Therefore, a single raw substrate material cannot be applied in any application due to lack of some properties. Each substrate has its own weakness like corrosion, hardness, wear, or something related to mechanical properties that need some treatment to enhance its properties. For further improvements of the substrate, it needs to proceed with some surface treatment like thermal spraying, PVD, electrodeposition and plasma spraying. All this method will help to improve each of the substrate properties based on its characterization.

2.5 Properties of Composite Coatings

In their research, on microstructure and properties of composite coatings, Zhang et al., (2018) highlight the significance of applying composite coatings in surface treatment to enhance the wear, corrosion, and oxidation resistance of substrate materials. They emphasize that various methods can be employed to improve the properties of composite coatings and specifically opt for plasma spraying technology due to its cost-effectiveness. Similarly, in their research, Zhou et al., (2018) communicate that they employed laser cladding and laser remelting techniques to enhance both the microstructure and corrosion resistance of amorphous composite coatings reinforced with tungsten carbide (WC). Their chosen methods aim to investigate the experimental process that could influence the microstructure and corrosion resistance of the composite coatings. Consequently, their research involves observing the microstructure of the coating and conducting corrosion tests to examine the properties of the coatings.

2.5.1 Hardness

In their investigation into the hardness and tribological characteristics of co-electrodeposited Ni-W-B/B, Harachai et al., (2020) found that a higher boron content contributes to an elevation in hardness in the Ni-W-B/B composite coatings. The sample, synthesized at a bath temperature of 75 °C with a boron addition of 5 g/L, demonstrated a peak hardness of 680.9 HV. However, when the loading of amorphous boron was increased to 10 g/L, the hardness exhibited a notable decrease. In binary alloy systems such as Ni-W or Ni-B, the incorporation of W or B aims to enhance the mechanical properties of the Ni coating by diminishing grain size an occurrence known as the Hall-Petch effect. This effect involves smaller grains impeding dislocation motions, thereby resulting in increased hardness. Within ternary alloy systems like Ni-W-B and Ni-W-P, the incorporation of a third component aims to enhance corrosion resistance. Although certain studies suggest a reduction in the grain size of Ni-W-B coatings with elevated W and B contents, resulting in heightened hardness, the inclusion of amorphous particles was observed to amplify the hardness of Ni-W-B coatings across all loading levels. This contrasts with the hardness observed in pure Ni-W-B films. In a separate study by Demir et al., (2020) on the

characterization of Ni-Cr/hBN composite coatings, the focus was on the hardness of the coatings. The Ni-Cr coating exhibited a hardness of 1.85 GPa, with a modulus of elasticity of 121.36 GPa. Hardness and elastic modulus values increased with an increase in hBN concentration from 5 to 10 and 20 g/L, but they declined when the hBN rate was further increased to 30 g/L. This decline was attributed to the agglomeration of hBN nanoparticles during the coating process and the challenges associated with the transport of agglomerated hBN nanoparticles by Ni-Cr ions during the electrodeposition process. A low modulus of elasticity suggested poor adherence between the coating and the substrate, resulting in reduced wear resistance. Microhardness testing corroborated the nanoindentation results, with a sample containing 538 HV and 20 g/L hBN demonstrating maximal hardness. Overall, the inclusion of hBN in the composite coatings showed a positive effect on hardness levels compared to the Ni-Cr alloy coating.

A finding done by Hamidi et al., (2021) on the effect of current density and bath temperature to the corrosion and wear behaviour of WC-Ni electrodeposition coating resulting that the current density influences the hardness of the composite coatings. It resulted where the increasing in current density and temperature, the hardness of coating is improve based on their experimental result. From their result, the increasing current density displays the largest percentage value around 23%, when compared to temperature increase, that is just 2%. The influence of current density and temperature might affect the hardness properties of composite coatings. Sharhida Othman et al., (2020) In their study, they investigated the impact of saccharin on the hardness properties of nickel-quarry dust composite coatings. They observed an increase in microhardness with a corresponding rise in the saccharin content. It is due to the crystallite size where the crystallite size is related to the microhardness. From their experimental, hardness rose linearly from about 260 HV for Ni-QD coating with the biggest grain size of 20 nm to approximately 350 HV for coating with the lowest grain size of 15 nm. The reduction of nanocrystalline materials' grain size resulted in an improvement in hardness. Therefore, the size of grain size closely related to the hardness where the small area of grain size input a large value of hardness.

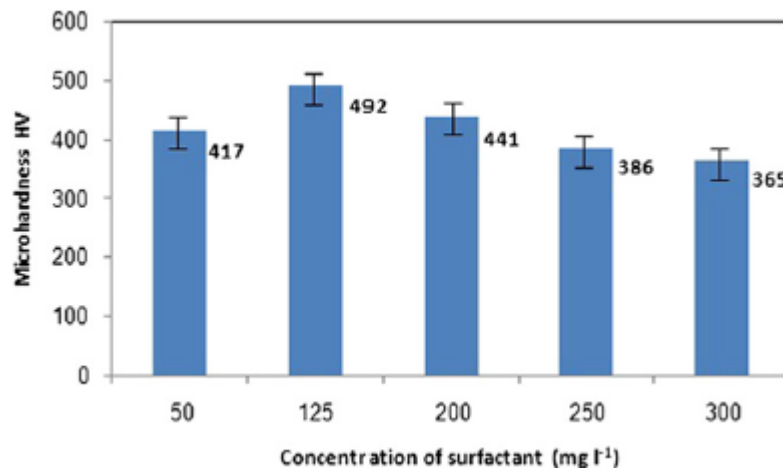


Figure 2.1: Hardness value of Ni-Al Coatings on the SDS effects (Sabri et al., 2012a)

2.5.2 Wear resistance

In their study on the wear behaviour of electrodeposited nickel/graphene composite coatings, Li et al., (2021) highlight the remarkable mechanical and tribological properties of graphene. Graphene exhibits inherent strength of up to 130 GPa, surpassing that of steel by more than 100 times, and a coefficient of friction comparable to or lower than graphite. Consequently, the addition of graphene enhances not only the lubricity of the metal matrix composite coating but also its wear resistance. According to their experimental findings, the friction coefficients of nickel coating and nickel/graphene composite coating exhibit similar trends, with friction coefficients becoming more stable as the distance increases. The friction coefficient of the nickel/graphene composite coating is reduced compared to the nickel coating, maintaining an average value of 0.16 after stabilization. In contrast, the friction coefficient of the pure nickel coating varies significantly. The friction coefficient of the nickel/graphene composite coating is reduced by 63.6% compared to the average friction coefficient of 0.44 for the stable nickel coating. The roughness of the nanocomposites plays a crucial role in influencing their wear resistance.

In their research, Zhang et al., (2019) highlighted the versatile applications of Ni-W coatings in aggressive environments, including aerospace, electronics, machinery, energy, and marine. These coatings are renowned for their exceptional wear resistance, stability, high hardness, low coefficient of thermal expansion, high corrosion resistance, antifriction properties, and magnetic characteristics, positioning them as a promising and

environmentally friendly substitute for hard chromium films. Despite the notable attributes of Ni-W coatings, the pursuit of improved performance has driven researchers to further explore their characteristics. The researchers observed a significant impact of tungsten content on the hardness, grain size, and structure of Ni-W coatings, ultimately influencing their overall performance. Experimental findings regarding wear properties revealed that Ni-W-GO coatings displayed a lower coefficient of friction (COF) compared to Ni-W coatings without graphene oxides (GOs). Throughout the testing, the COF initially increased to a specific value, underwent variations, and eventually stabilized at a constant level, with consistent friction behaviours observed in all presented Ni-W-GO composite coatings. Additionally, the COF decreased with an increase in GO concentration, reaching a minimum of approximately 0.55 when the bath contained 0.15 g/L GOs. The dispersion of sufficient GOs in the plating bath improved the coating's resistance to local deformation, provided numerous nuclei, and increased the number of grains, resulting in dual hard particle and fine grain strengthening effects in the Ni-W-GO coating. Isolated from the matrix, GOs exhibited strong wear resistance and a self-lubricating effect, serving as solid lubricants to reduce direct contact between two wear surfaces and lower the overall wear rate of the composite coatings. The wear resistance of the Ni-W-GO composite coating was significantly enhanced due to the presence of GOs in the study. Both the coefficient of friction (COF) and microhardness played crucial roles in influencing wear performance. Therefore, the wear behaviour of the composite coatings was intricately linked to microstructural features and grain size. The improvement in wear resistance was also associated with experimental parameters such as current density, pH value, temperature, and surfactant content. A comprehensive study of coating material properties is essential to ensure that the applied treatment effectively enhances wear properties.

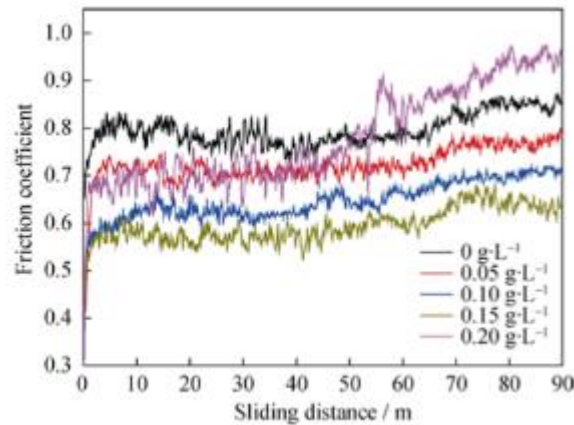


Figure 2.2: COF value of Ni-W-GO composite coatings (X. H. Zhang et al., 2019)

2.5.3 Corrosion Resistance

Jiang et al., (2018) on their research focus on the improvement of corrosion resistance on Ni-SiC composite coatings. They are focusing on boosting NdFeB corrosion resistance by adding alloy components, which can also reduce magnetic properties. They also want to employ electrodeposition to protect the surface of the magnet. In another variant involving mixed particles, nickel is utilized as the matrix metal, and silicon carbide (SiC) is dispersed throughout the solution. The Ni-SiC composite coating is created by simultaneously depositing SiC particles and nickel ions through electrodeposition. The result from their experimental shows that the capacitive loop radius of the Ni-SiC coating was greater than that of the pure nickel coating, however the capacitance maximum arc radius of the magnetic field enhanced jet electrodeposition Ni-SiC coating is smaller. The corrosion resistance increased as the radius increased, and the polarisation resistance increased. As a result, Ni-SiC coating significantly increased coating corrosion resistance, and magnetic field jet electrodeposition can further improve it. He et al., (2018) in their research they aimed the pulsed electrodeposition technique that used to create Ni-W-B₄C composite coatings, and the influence of B₄C nanoparticle reinforcement on the microstructural, micro-hardness, and corrosion resistance characteristics of the composite coatings is examined. The experimental results reveal that the corrosion resistance of the composite coatings is affected by B₄C. This is demonstrated by the superior corrosion resistance observed in the deposited Ni-W-B₄C coatings as compared to Ni-W coatings. B₄C content cannot exceed 2 g/L because this content of B₄C is the optimum level and if it exceeds the limit the performance of corrosion

resistance of the composite coating will be drop. The influence of B_4C content control the corrosion resistance properties of the composite coatings. Therefore, there are two main reason which enhancing the corrosion resistance in the experiment. The first one is doping B_4C nanoparticles into Ni-W alloy coatings not only refines the grain, smoothens and uniformizes the coating, but also acts as a physical barrier layer, preventing corrosion. Second, the homogeneous dispersion of B_4C nanoparticles improves coating strength and inhibits matrix dissolution, considerably improving coating corrosion resistance.

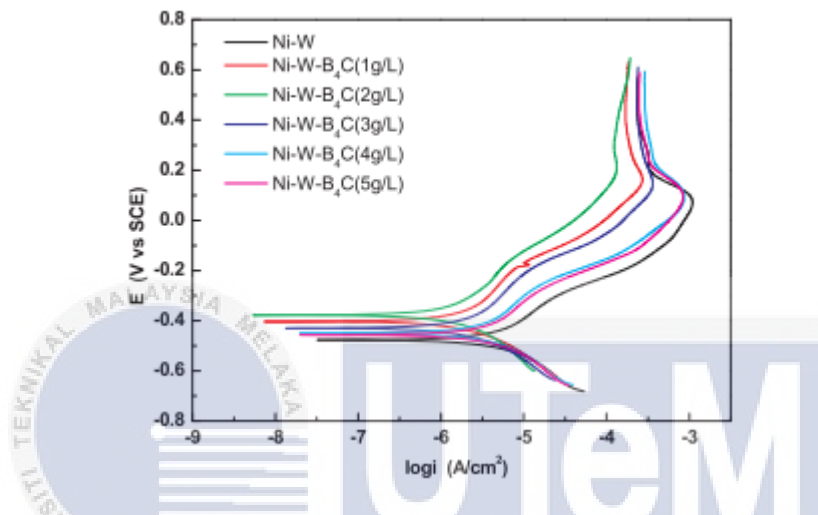


Figure 2.3: The polarization curve of Ni-W alloy with Ni-W- B_4C composite coatings (He et al., 2018)

CHAPTER 3

METHODOLOGY

This chapter centres on detailing the approach employed for the electrodeposition current density process of Ni-Recycled quarry dust composite coatings. The experiment encompasses sample preparation, quarry dust preparation, the electrodeposition process, as well as surface characterization and mechanical testing conducted on the coated substrate.

3.1 Overview

To complete the experiment, a flow chart has been created to overview the process flow. The experiment begins with the preparation of the substrate sample, including cutting and grinding processes. Following this, quarry dust is crushed to obtain fine particles through a sieving process. The preparation of the nickel's Watt bath occurs next, setting the stage for the electrodeposition process where the appropriate current density is applied. During this process, quarry dust and sodium dodecyl sulphate (SDS) surfactant are added at the required concentrations.

Once the electrodeposition process is completed, the coated substrate undergoes surface morphology scanning. To analyse the surface characteristics of the coated substrate, tools such as SEM and XRD machines are employed. The final stage involves conducting tests for micro-hardness, wear, and corrosion. The micro-hardness test is performed using a micro-Vickers machine, while the wear test is conducted using a pin-on-disc machine. All testing adheres to the standards set by the American Society for Testing and Materials (ASTM). Figure 3.1 presents the flowchart of the experimental procedure.

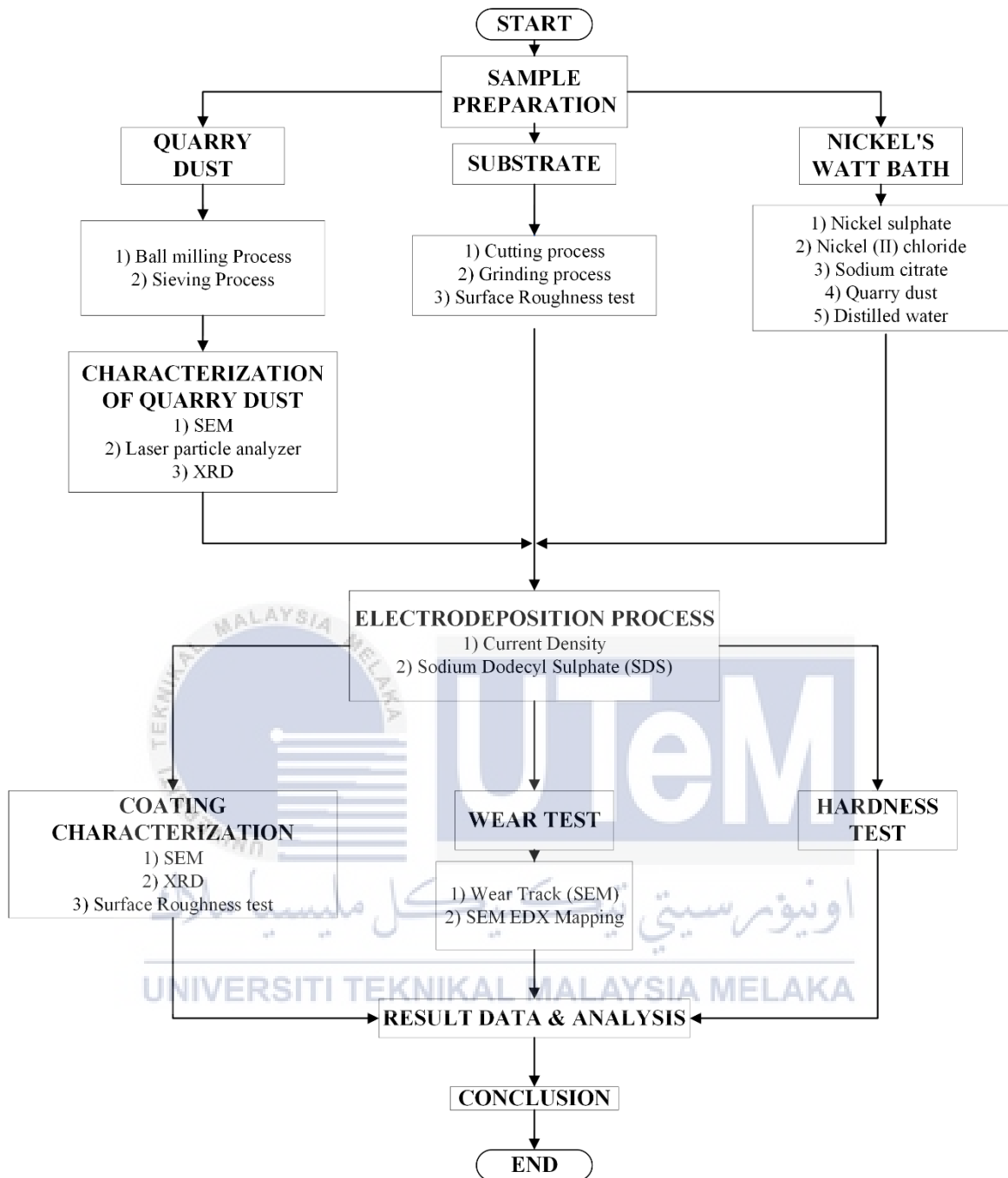


Figure 3.1: Flowchart of the experimental procedure

3.2 Substrate preparation

The substrate used in this experiment is mild steel, which readily rusts in the presence of water and oxygen from the environment. This steel requires specific treatment to address its surface property weaknesses. To enhance its characteristics, the steel undergoes an electrodeposition procedure to coat its surface. Before initiating the electrodeposition process, the steel is cut into small pieces to facilitate the procedure and ground to achieve a fine and smooth surface. The cutting process is conducted at the FTKIP Welding Lab using a laser cutting machine. Figure 3.1 below shows an example of a mild steel plate.

3.2.1 Substrate cutting

In this experiment, mild steel is employed as the substrate. The mild steel is cut into 25 rectangular sample pieces, each measuring 40mm x 30mm x 3mm. Figure 3.2 below shows the dimensions of the mild steel substrate.

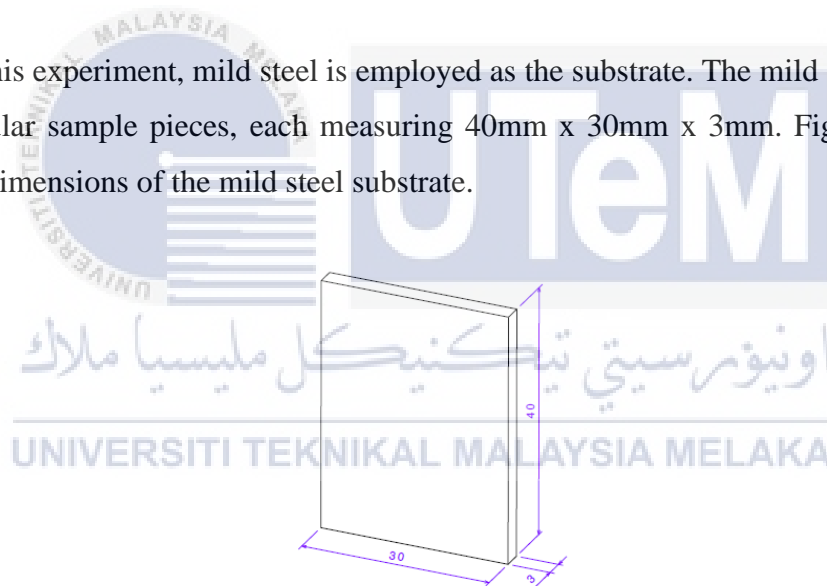


Figure 3.2: Dimension of the mild steel substrate

3.2.2 Substrate Grinding and polishing

After cutting the substrate into pieces, the grinding process is conducted to ensure the surface is smooth enough to begin the electrodeposition process. Abrasive paper with grits of 240, 400, 600, 800, and 1200 is used on the grinding machine to remove oxides. The

grinding machine operates at a speed of 200 rpm to ensure the substrate surface is adequately ground and smooth. Figure 3.3 shows the grinding machine used to grind the substrate.



Figure 3.3: Grinding machine

3.3 Quarry dust preparation

The acquired quarry dust is processed using the laboratory's planetary ball mill equipment. After the milling operation, the quarry dust powder is sieved to achieve a fine and smooth size.

3.3.1 Quarry dust mill process

The quarry dust is milled using the planetary ball mill machine for 20 minutes at a speed of 400 rpm. Steel balls and a steel jar are used in this experiment. Figure 3.5 shows the PM100 planetary ball mill machine used to mill the quarry dust.



Figure 3.4: Planetary ball mill machine, PM100

3.3.2 Quarry dust sieving process

After the quarry dust milling process is completed, the milled quarry dust is sieved to separate larger particles and produce a fine-sized quarry dust powder. A sieve with a mesh size of $63\mu\text{m}$ is utilized in this procedure to sieve the milled quarry dust. Fine-sized quarry dust particles are employed in the electrodeposition procedure because they disperse more easily in the nickel's Watt bath solution than larger particles. Figure 3.5 shows the octagon siever machine used to sieve the milled quarry dust.



Figure 3.5: Octagon siever machine

3.4 Electrodeposition process

The cleaned mild steel substrate will undergo the electrodeposition process. In the electrolyte, the substrate will be placed as the cathode and the nickel plate as the anode. The electrodeposition procedure will utilize a direct current (DC) source. Figure 3.6 shows the setup of the electrodeposition process.

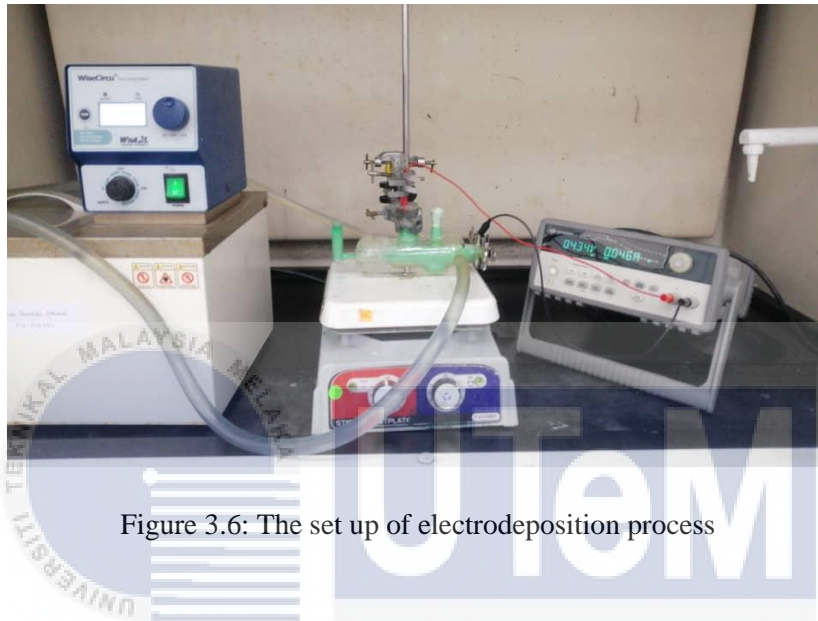


Figure 3.6: The set up of electrodeposition process

3.4.1 Nickel's watt bath

The electrolyte solution in the nickel's watt baths consist of Nickel sulphate ($\text{NiSO}_4(\text{H}_2\text{O})_6$), Nickel (ii) chloride (NiCl_2), Sodium chloride (NaCl), sodium citrate, and sodium tungstate. The concentration of each chemical is given in the Table 3.1 below and the operating condition is provided in Table 3.2.

Table 3.1: Concentration of chemical in nickel's watt bath

Chemical	Concentration (g/L)
Nickel sulphate, NiSO_4	100
Nickel (ii) chloride, NiCl_2	20
Sodium citrate, $\text{Na}_3\text{C}_6\text{H}_5\text{O}_7$	15
Quarry dust	40
SDS	0, 0.25, 0.50, 0.75, 1.0

Table 3.2: Electrodeposition operating condition table

Operating Condition	
Stirrer (rpm)	200
Current density (A/dm ²)	1,3,5,7,9
Duration (min)	60
Temperature (° C)	40

3.4.2 Electrodeposition Parameters

In the electrodeposition process, current density plays a critical role in controlling the amount of current applied in the electrolyte, thereby influencing the experimental outcomes. Sodium dodecyl sulphate surfactant (SDS) is added to the electrolyte to aid in the dispersion of quarry dust in the nickel Watt's bath solution. The concentration of SDS also impacts the experimental results. Table 3.3 below presents the parameters of current density and sodium dodecyl sulphate surfactant (SDS) content used in this process.

Table 3.3: Experiment parameter table

Current density (A/dm ²) \ SDS content (g/L)					
	1	3	5	7	9
0	S1	S2	S3	S4	S5
0.25	S6	S7	S8	S9	S10
0.50	S11	S12	S13	S14	S15
0.75	S16	S17	S18	S19	S20
1.0	S21	S22	S23	S24	S25

3.5 Material Characterization

SEM and XRD techniques were utilized to examine the morphology of composite coatings containing Ni-W and recycled quarry dust on the coated substrate. The scanning electron microscope (SEM) and X-ray diffraction (XRD) machine analysed the morphology and structure of the quarry dust. Furthermore, a particle size analyser (PSA) was used to measure the particle size of quarry dust, enabling differentiation between sizes before and after the sieving process.

3.5.1 Scanning Electron Microscope machine (SEM)

In this experiment, a scanning electron microscope (SEM, ASTM E986) is employed to evaluate and analyse the morphology of the coated substrate. SEM can provide detailed information about the surface morphology and chemical composition of the material. Figure 3.7 depicts the scanning electron microscope machine used for the characterization of the coated substrate.

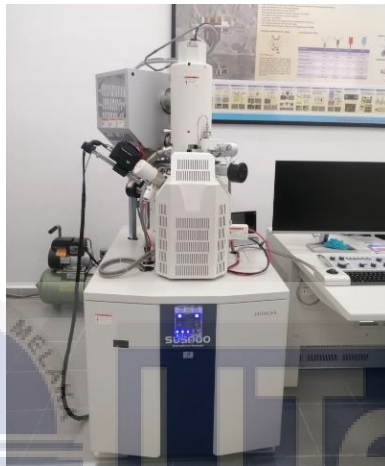


Figure 3.7: Scanning Electron Microscope machine

3.5.2 X-ray Diffraction machine (XRD)

X-ray diffraction (XRD) is a non-destructive method used to characterize crystalline materials. It provides detailed information on crystal structures and structural parameters such as crystallinity, average grain size, and crystal defects. In this experiment, the XRD machine will be used to observe the crystal structure and grain size of Ni-W-Recycled quarry dust. Figure 3.8 illustrates the X-ray diffraction machine (XRD). The crystallite size will be calculated using the Scherrer equation, as shown in Equation 3.1 below.

$$\text{scherrer equation} = \frac{K\lambda}{\beta \cos \theta} \quad \text{Equation 3.1}$$



Figure 3.8: X-ray Diffraction Machine (XRD)

3.5.3 Particle Size Analyzer

Laser particle analysers are used to assess particle sizes in both liquid and powder forms. In this experiment, a particle size analyser is employed to evaluate the particle size of quarry dust before and after the milling process. This equipment provides data on particle size and can distinguish between particle sizes before and after the milling procedure.

3.6 Sample Testing

In this experiment, mechanical testing is performed to assess the hardness, wear resistance, and corrosion resistance of each coated sample. The micro-Vickers hardness test will be conducted using a micro-Vickers hardness tester, while the wear test will be carried out using a pin-on-disc machine. The corrosion test will utilize electrochemical impedance spectroscopy (EIS).

3.6.1 Micro- hardness

The hardness tests at FKM AMCHAL Lab will be conducted using a micro-Vickers tester, with the indenter applied at various locations on the coated surface under a 100g load.

Each test will be performed for 15 seconds. Following the indentation process, the results will be analyzed by measuring the dimensions of the diamond shape to determine the hardness of the coated material. Figure 3.8 depicts the micro-Vickers machine used for the hardness test.



Figure 3.9: Microvickers machine (Hardness-test)

3.6.2 Wear test

The wear behavior of the coating will be analyzed using a pin-on-disc tester (DIN 50324-07, ASTM G99-05, ISO 18535) equipped with specialized equipment. This apparatus reciprocates a 10 mm stainless steel ball against the sample, applying a constant stress of 10N. The test parameters include a sliding speed of 5 mm/s, a stroke of 2.69 mm, and a duration of 1500 seconds. Assessment of the coating's wear behavior involves measuring the coefficient of friction (COF) generated during the reciprocating motion of the ball across the coated layer. Additionally, the wear track will be examined using both scanning electron microscopy (SEM) and a 3D profilometer. Figure 3.10 depicts the pin-on-disc machine used for the wear test.



Figure 3.10: Micro Pin on Disk Tribo Tester (CM-9109)



CHAPTER 4

RESULT & DISCUSSION

This chapter will discuss the experimental results. All data and findings obtained from the Particle Size Analyzer (PSA), X-ray Fluorescence (XRF), X-ray Diffraction (XRD), Scanning Electron Microscopy (SEM), Wear Test, and Hardness Test will be analyzed to determine the extent to which this experiment achieves its objectives.

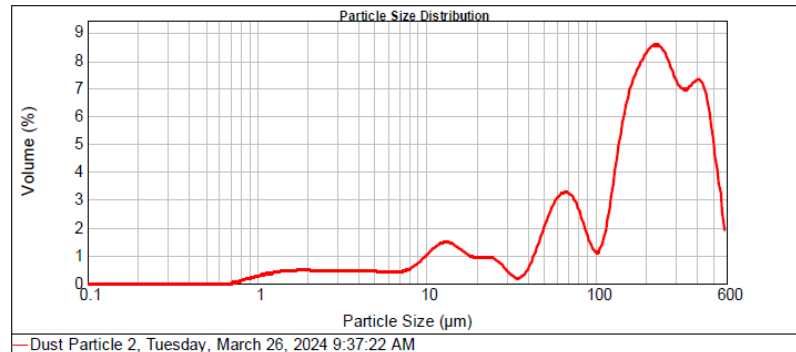
4.1 Characterization of Quarry Dust

4.1.1 Particle Size Analysis of Quarry Dust

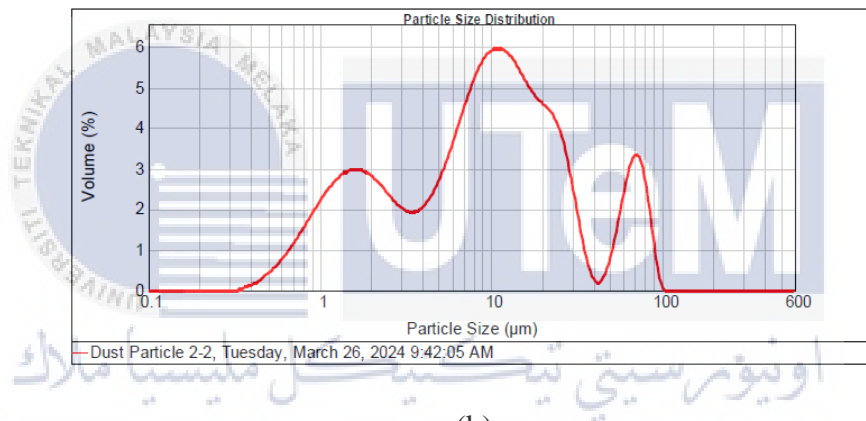
Figure 4.1 below shows the distribution of quarry dust particles using particle size analysis (PSA). The distribution highlights three different size categories: as received, after the ball milling process, and after the sieving process. The as-received quarry dust consists of large particles ranging from 0.724 μm to 630 μm . Based on Figure 4.1(a), the distribution indicates that most particles are within the range of up to 100 μm .

Figure 4.2(b) shows the distribution of quarry dust particles after a 5-hour ball milling process at 350 rpm. This process reduced the particle size to a range of 0.363 μm to 91.201 μm . Although the particles became powdery, they were still not fine enough and remained coarse, requiring the sieving process. The sieving process further refined the particles, using a 63 μm sieve for 28 minutes. Figure 4.1(c) shows the particle distribution

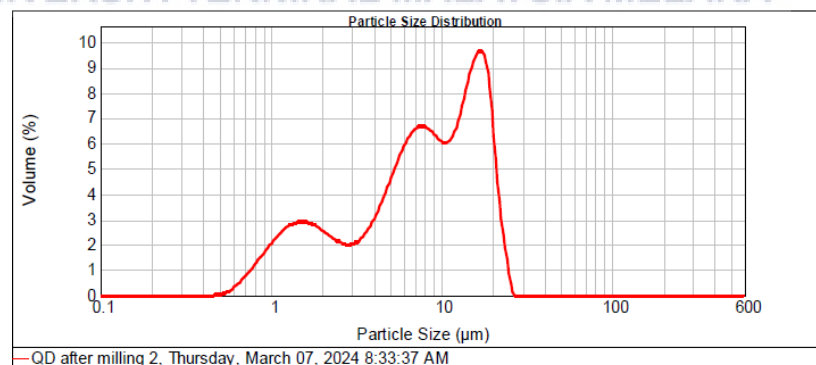
after sieving, targeting sizes between 1 μm and 63 μm . After sieving, PSA analysis confirmed that the particle sizes were below 63 μm .



(a)



(b)



(c)

Figure 4.1: The particle size distribution of quarry dust (a) as received (b) after ball milling process for 5 hours at 350 rpm (c) after sieve using 63 μm sieve pan.

4.1.2 Phase Analysis of Quarry Dust

X-ray Diffraction (XRD) was employed to identify the phase composition of quarry dust particles. Figure 4.2 shows the XRD results, indicating that the intensity peaks for alumina (Al_2O_3) and silica (SiO_2) are prominent. Silica (SiO_2) appears at higher intensity peaks compared to alumina (Al_2O_3), which shows up at smaller peaks. The presence of alumina and silica in the XRD results confirms that quarry dust particles are rich in these compounds, making them suitable as substitute materials for raw alumina and silica. This finding aligns with the research by Othman et al., (2019), which demonstrated that quarry dust particles are high in alumina and silica, especially after extended ball milling.

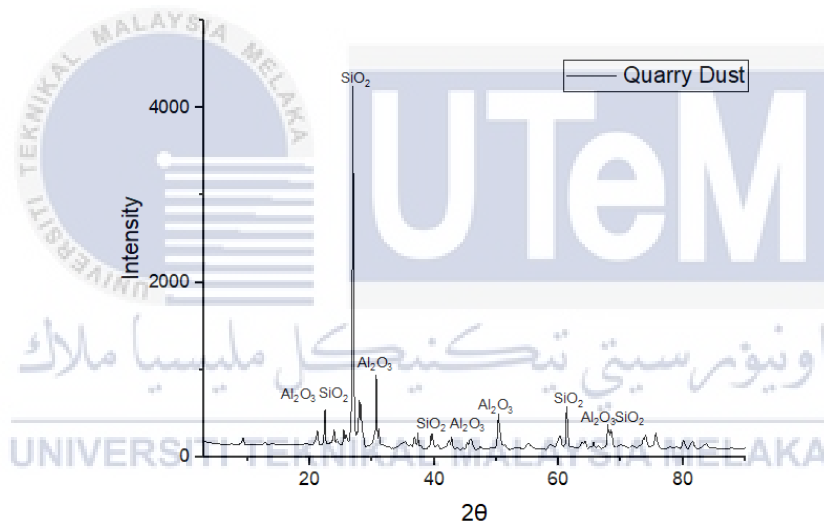
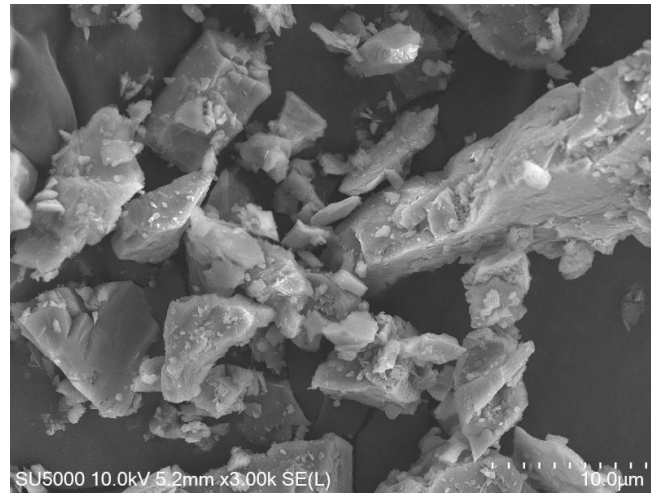


Figure 4.2: XRD analysis of quarry dust particles

4.1.3 Surface Morphology of Quarry Dust

Quarry dust particles were subjected to Scanning Electron Microscopy (SEM) to examine their morphology. Figure 4.3 (a) displays the surface morphology of the as-received quarry dust particles, which are irregular in shape and vary in size. Figure 4.3 (b) shows the morphology of the quarry dust particles after undergoing a ball milling process for 5 hours

at 350 rpm, followed by sieving for 28 minutes using a 63 μm sieve. After these processes, the particles remain irregular in shape, but their size is significantly finer.



(a)



(b)

Figure 4.3: SEM observation of quarry dust particles (a) as received (b) After 5 hours of ball milling with 350 rpm

4.1.4 X-Ray Fluorescence (XRF) of Quarry Dust

X-ray Fluorescence (XRF) analysis was conducted to determine the detailed composition of quarry dust particles. According to Figure 4.2, which presents the X-ray Diffraction (XRD) analysis, the peaks indicate that silica (SiO_2) and alumina (Al_2O_3) are the most prominent, with silica showing the highest intensity. This finding is corroborated by

the XRF analysis, confirming that silica (SiO_2) is the dominant element in the quarry dust, followed by alumina (Al_2O_3).

Table 4.1 details the elemental composition of the quarry dust, showing that silica (SiO_2) and alumina (Al_2O_3) are the primary components, comprising 72.6 wt.% and 15.1 wt.% respectively. Other elements present in the quarry dust include potassium oxide (K_2O), sodium oxide (Na_2O), ferric oxide (Fe_2O_3), calcium oxide (CaO), magnesium oxide (MgO), titanium dioxide (TiO_2), sulfur trioxide (SO_3), and phosphorus pentoxide (P_2O_5), each constituting less than 5 wt.% of the total composition. Figure 4.3 displays a pie chart illustrating the elemental composition of the quarry dust, highlighting silica and alumina as the dominant elements.

Table 4.1: Element composition in quarry dust particles

Element	Concentration (wt.%)
Silica (SiO_2)	72.6
Alumina (Al_2O_3)	15.1
Potassium Oxide (K_2O)	4.9
Sodium Oxide (Na_2O)	3.0
Ferric Oxide (Fe_2O_3)	1.9
Calcium Oxide (CaO)	1.1
Magnesium Oxide (MgO)	0.8
Titanium Dioxide (TiO_2)	0.3
Sulphur Trioxide (SO_3)	0.2
Phosphorus Pentoxide (P_2O_5)	0.1

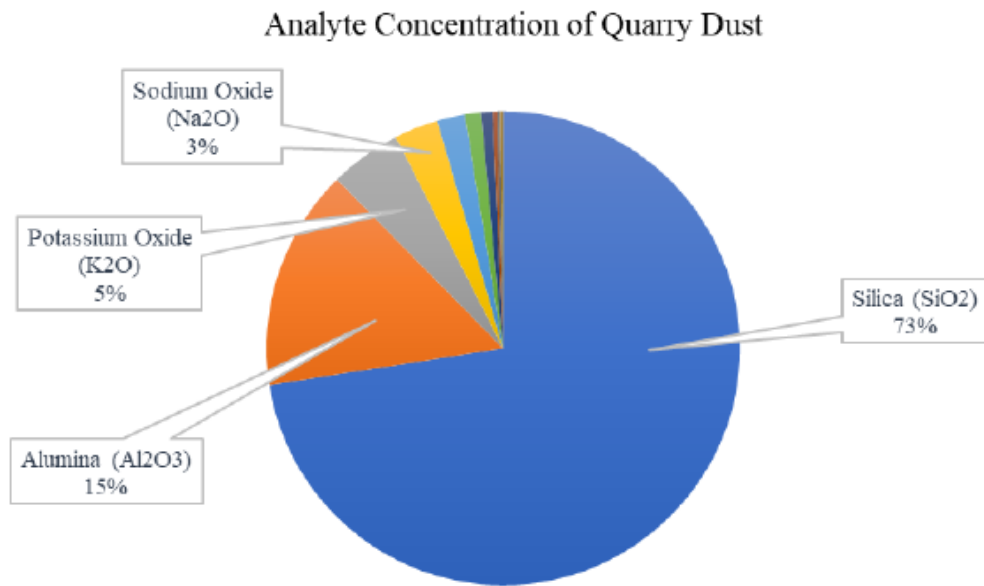
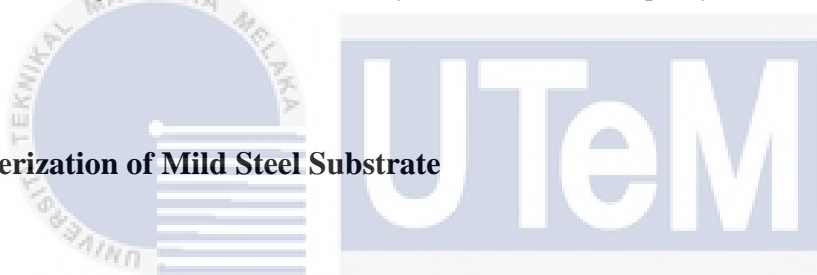


Figure 4.4: Pie chart of analyte concentration of quarry dust through XRF



4.2 Characterization of Mild Steel Substrate

4.2.1 Energy Dispersive X-ray of Mild Steel Substrate

The sample substrate, which is mild steel, was subjected to Energy Dispersive X-ray (EDX) analysis to determine its elemental composition. Figure 4.5 presents the EDX spectrum of the mild steel substrate, revealing the presence of three elements: iron (Fe), carbon (C), and oxygen (O). Table 4.2 below summarizes the elemental composition of the mild steel substrate, showing that it is predominantly composed of iron (Fe) at 76.9 wt.%, followed by carbon (C) at 20.1 wt.%, and oxygen (O) at 3.0 wt.%.

Sum Spectrum

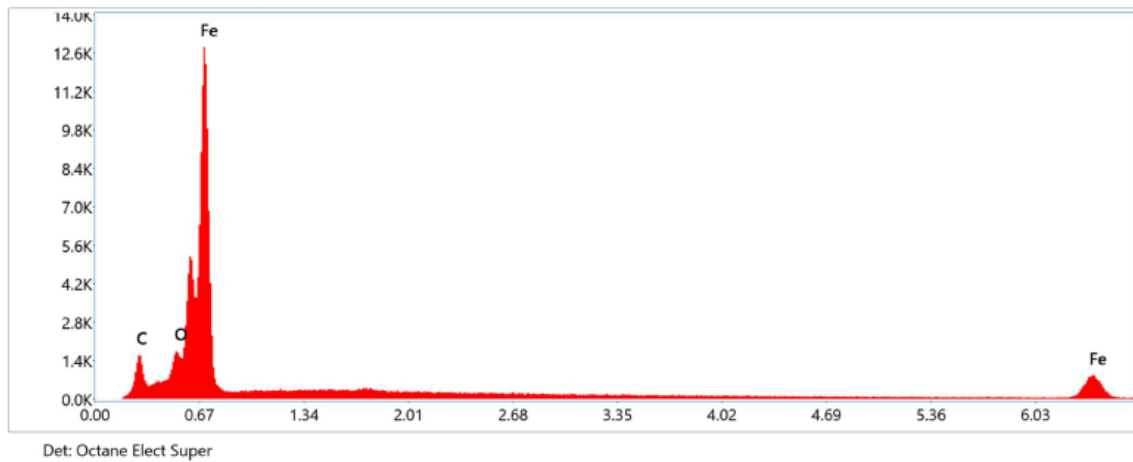


Figure 4.5: EDX spectrum of mild steel substrate

Table 4 2: Element composition of mild steel substrate

Element	Composition (wt. %)
Iron (Fe)	76.9
Carbon (C)	20.1
Oxide (O)	3.0

4.2.2 Surface Roughness of Mild Steel Substrate

The surface roughness test was conducted on the mild steel substrate to evaluate its roughness after the grinding process. Figure 4.6 shows the surface roughness of the mild steel substrate, with the average roughness for the five tested samples being 29.38 μm .

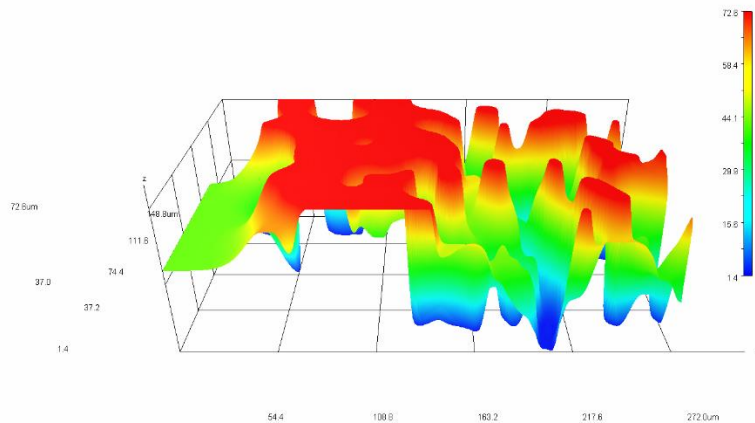



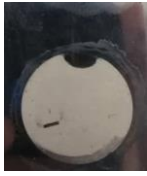



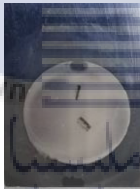









Figure 4.6: Surface roughness of substrate

4.3 Characterization of Nickel-Quarry Dust Composite Coatings

4.3.1 Visual Inspection of Nickel-Quarry Dust Composite Coatings

Table 4.3 presents the completed samples that were electrodeposited using various current densities and sodium dodecyl sulfate (SDS) contents. Out of 25 samples, 20 were successfully coated, while 5 samples (samples 10, 19, 20, 24, and 25) failed to coat due to solution overflow during the experimental process. Figure 4.7 illustrates the solution overflow during the electrodeposition process caused by the high SDS content and current density.

Table 4. 3: Experiment result

Current density (A/dm ²) SDS content (g/L)	1	3	5	7	9
0					
	SAMPLE 1	SAMPLE 2	SAMPLE 3	SAMPLE 4	SAMPLE 5
0.25					
	SAMPLE 6	SAMPLE 7	SAMPLE 8	SAMPLE 9	SAMPLE 10
0.50					
	SAMPLE 11	SAMPLE 12	SAMPLE 13	SAMPLE 14	SAMPLE 15


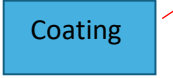


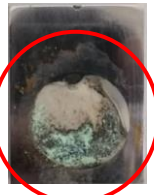
0.75							
			SAMPLE 16	SAMPLE 17	SAMPLE 18	SAMPLE 19	SAMPLE 20
1.0							
			SAMPLE 21	SAMPLE 22	SAMPLE 23	SAMPLE 24	SAMPLE 25



Figure 4.7: Solution overflow during electrodeposition process

4.3.2 X-ray Diffraction of Nickel – Quarry Dust Composite Coatings

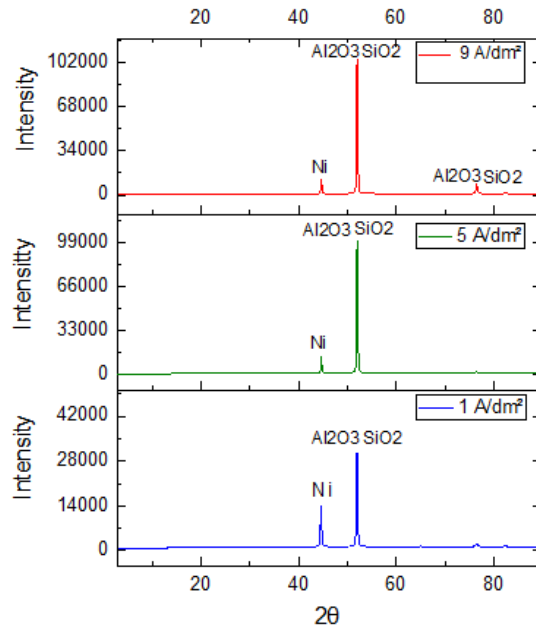
XRD analysis was utilized to determine the phase composition of the nickel-quarry dust composite coatings. Figure 4.8 (a) and (b) show the XRD patterns for the composite coatings with and without SDS surfactant at various current densities. Figure 4.8 (a) illustrates the XRD results for the coatings without SDS surfactant. The highest peaks are

dominated by alumina (Al_2O_3) and silica (SiO_2) present in the quarry dust at a theta angle of 51° . These results confirm the successful incorporation of quarry dust particles into the composite coatings. As the current density increases, the intensity of the alumina and silica peaks also increases due to rapid deposition during the electrodeposition process. Nickel (Ni) particles are also present in the XRD results at a theta angle of 45° , but with lower intensity compared to alumina and silica. The intensity of the nickel peaks increases with higher current density, attributable to the higher deposition rate during the electrodeposition process.

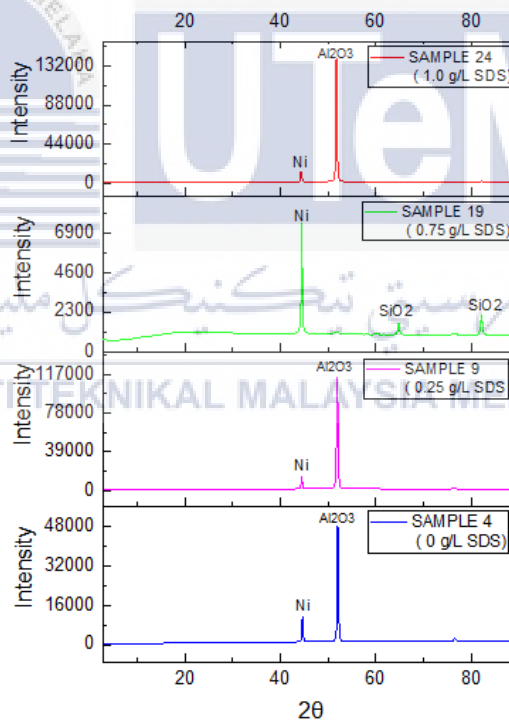
Figure 4.8 (b) shows the XRD results of nickel-quarry dust composite coatings at a current density of 7 A/dm^2 with varying SDS content. As the SDS content increases from 0 g/L to 0.25 g/L , the elements identified are alumina (Al_2O_3), silica (SiO_2), and nickel (Ni). Alumina and silica dominate the XRD patterns with higher intensity compared to nickel, facilitated by the SDS surfactant's role in uniformly distributing nickel, alumina, and silica particles during the electrodeposition process. Alumina and silica peaks appear at a theta angle of 51° , while nickel peaks are observed at 45° .

When the SDS content is increased from 0.25 g/L to 0.75 g/L , no alumina is detected in the XRD results. This absence is attributed to the overflow of the solution during the electrodeposition process, caused by the interaction between the high current density of 7 A/dm^2 and the elevated SDS content of 0.75 g/L . Figure 4.7 illustrates the solution overflow during the experiment, which led to the termination of the process and the experiment being deemed unsuccessful. Despite this, the sample was analysed via XRD to check for the presence of alumina, silica, and nickel elements. The XRD results revealed the presence of nickel and silica, likely due to the brief duration of the electrodeposition process before the overflow occurred.

As the SDS content increases from 0.75 g/L to 1.0 g/L , alumina and nickel elements are present, but no silica is detected. Like the sample with 0.75 g/L SDS content at a current density of 7 A/dm^2 , the experiment with 1.0 g/L SDS content at the same current density also had to be stopped due to solution overflow, as shown in Figure 4.7.



(a)



(b)

Figure 4.8: The XRD result of nickel- quarry dust composite coatings (a) Without SDS surfactant and various current density and (b) 7 A/dm² current density and various SDS content

4.3.3 Surface Morphology of Nickel-Quarry dust composite coatings

Scanning Electron Microscopy was used to examine the surface morphology of nickel-quarry dust composite coatings. Figure 4.9 shows the surface morphology of these coatings with 0.50 g/L SDS content at various current densities. Figure 4.9 (a) depicts the small, uniform, and compact grain size of the nickel-quarry dust particles deposited at 1 A/dm², attributed to the low current density and medium SDS content. As the current density increases to 5 A/dm², the grain size starts to agglomerate and appears bumpy, as shown in Figure 4.9 (b). At this stage, the rapid deposition of nickel-quarry dust particles due to the higher current density leads to an increase in grain boundaries on the coating.

In Figure 4.9 (c), the grain size of the nickel-quarry dust particles becomes larger, more agglomerated, stacked, and bumpy. The rapid deposition process, driven by the high current density, results in more nickel and quarry dust particles being deposited. This observation is supported by research from Boukhouiete et al., (2021) which states that increasing the current density can enlarge the grain size of the coating. At lower current densities, the coating takes more time to achieve the desired thickness, allowing more time for particles to accumulate at the cathode. Conversely, high current densities increase the deposition rate but make it difficult to control the deposition process.

Figure 4.10 shows the surface morphology of nickel-quarry dust composite coatings at a current density of 5 A/dm² with varying SDS content. As the SDS content increases, the grain size of the nickel-quarry dust composite coatings becomes more controlled, preventing over-deposition due to the high current density. Figure 4.10 (a) illustrates the surface morphology without SDS surfactant, revealing stacked and non-uniform grain sizes. With the addition of SDS, as shown in Figures 4.10 (a) at 0.50 g/L, (b) at 0.75 g/L, and (c) at 1.0 g/L, the grain size appears more uniform, agglomerated, bumpy, and stacked. This improvement is due to the presence of the SDS surfactant, which helps achieve a more uniform and well-distributed deposition.

Guo et al. (2018) observed that the addition of SDS results in a more defined cauliflower-like grain shape. They explained that SDS acts as an effective foaming agent for nickel electrodeposition, generating numerous small hydrogen bubbles on the cathodic surface that detach, leading to a specific morphological deposition. Comparing Figures 4.9 (a), (b), and (c) demonstrates that the presence of SDS surfactant helps control the deposition

rate at high current densities, resulting in a more uniform and controlled grain size. A similar effect is observed in Figures 4.10 (a), (b), (c), and (d), where the uniformity of the deposited quarry dust particles varies with and without SDS surfactant.

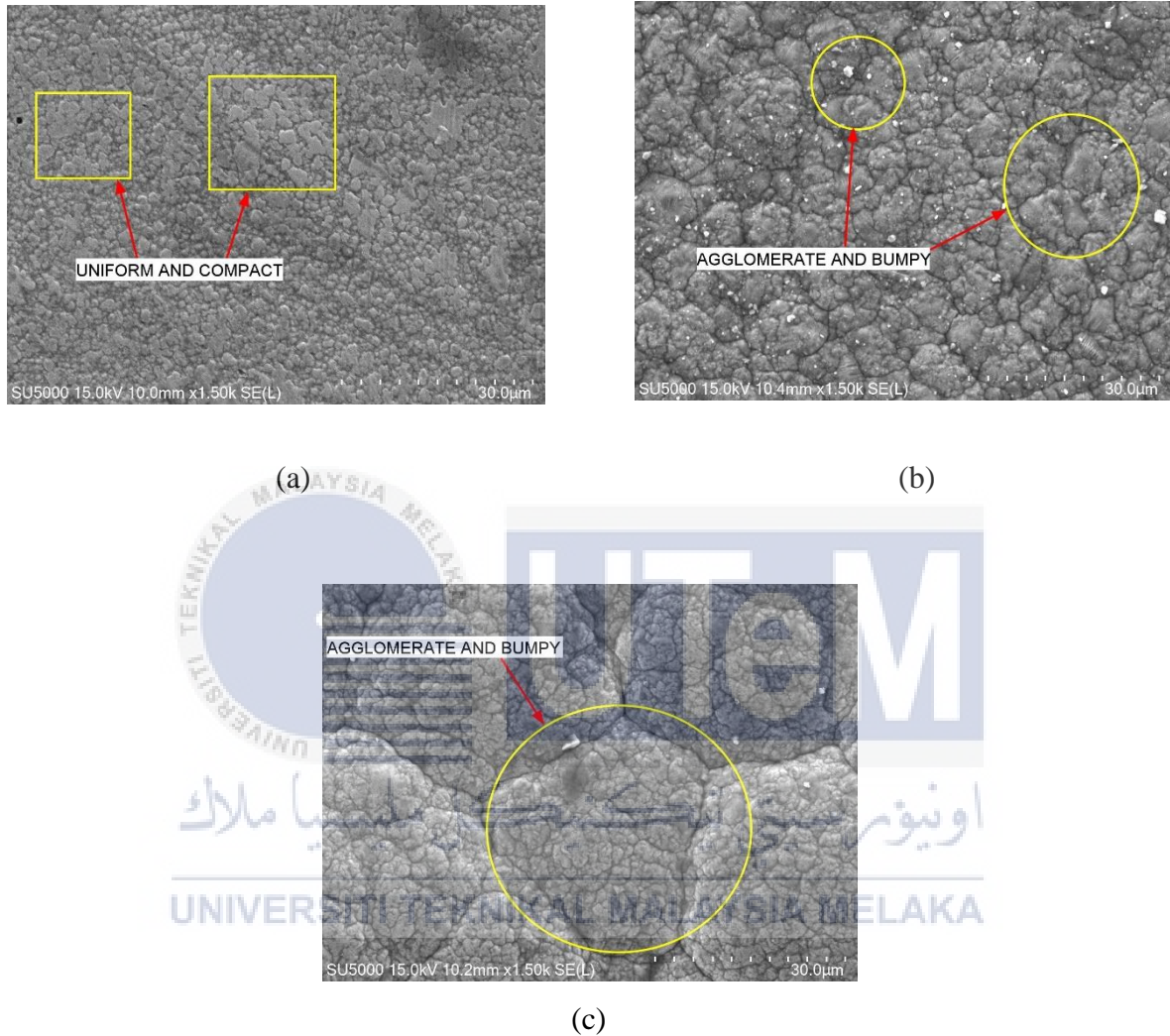


Figure 4.9: Surface morphology of nickel-quarry dust composite coatings produce using 0.50 g/L SDS at various current density with (a) 1 A/dm² (b) 5 A/dm² and (c) 9 A/dm² current density

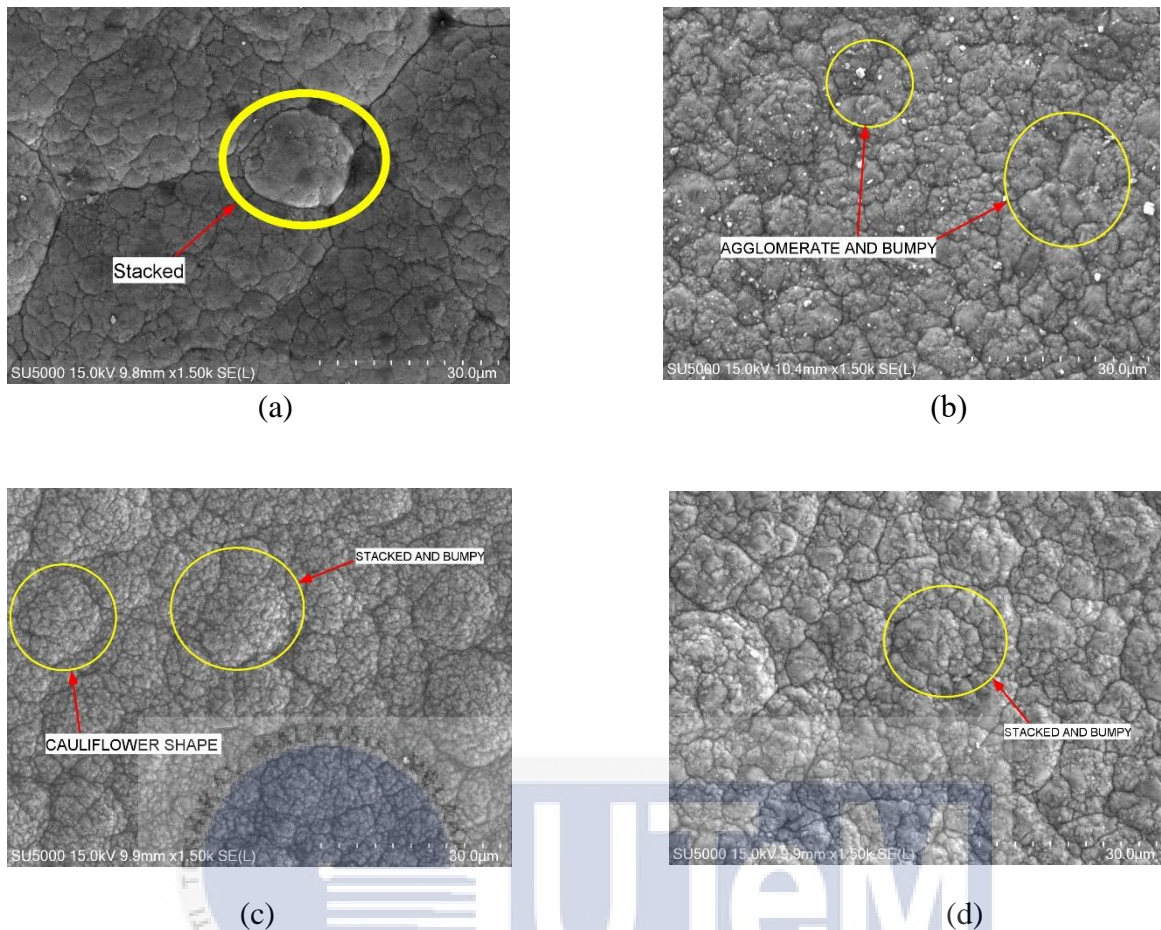


Figure 4.10: Surface morphology of nickel-quarry dust composite coating produce at 5 A/dm² of current density with various SDS content (a) 0 (b) 0.50 (c) 0.75 (d) 1.0 g/L

4.3.4 Surface Roughness of Nickel-Quarry Dust Composite Coatings

A surface roughness test was conducted to determine the roughness of the composite coatings. However, not all samples underwent this test due to time limitations. As shown in Figure 4.11, the surface roughness of nickel-quarry dust composite coatings increases with the current density, attributed to the high deposition rate during the electrodeposition process. Additionally, as the SDS content increases, the surface roughness also rises due to the uniformity of deposition. However, at high current density (9 A/dm²) and high SDS (0.50 g/L) content, the surface roughness increases significantly, resulting in a rougher surface compared to other conditions.

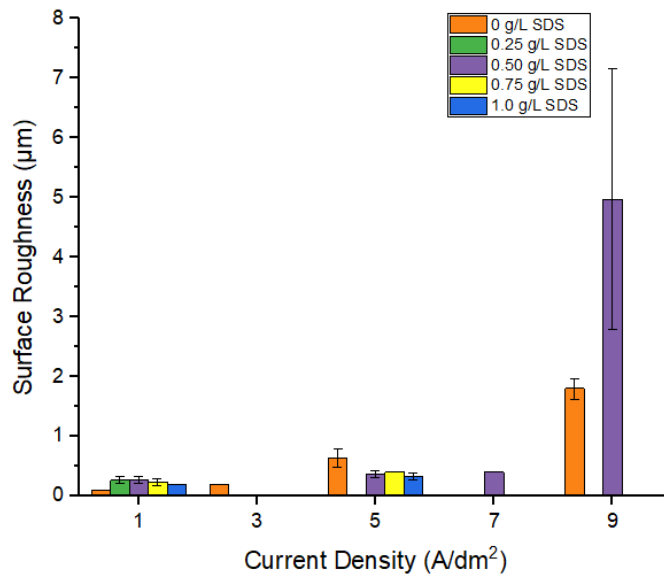


Figure 4.11: Surface roughness of nickel-quarry dust composite coatings

4.4 Nickel-Quarry Dust Composite Coating Test

4.4.1 Hardness Test on The Nickel-Quarry Dust Composite Coatings

The hardness test was conducted to examine the hardness properties of nickel-quarry dust composite coatings. Figure 4.12 shows the hardness results of these coatings. As the current density increases from 1 A/dm² to 3 A/dm², the hardness properties also increase due to the increased thickness of the deposited coatings. However, as the current density increases further from 3 A/dm² to 9 A/dm², the hardness properties remain constant, indicating that the optimum current density value is 3 A/dm², as there is no significant difference in hardness beyond this point.

This finding consistent with a study by Rosyidan et al., (2024) who found that the increase in hardness value with current density is attributed to the thickness and grain size of the composite coatings. During the electrodeposition process, a higher current density leads to a greater distribution of particles, resulting in the growth of nickel-quarry dust grain size and thickness, which in turn increases the hardness value.

Figure 4.12 also shows the effect of SDS surfactant on the hardness properties of nickel-quarry dust composite coatings. At current densities of 1 A/dm² and 3 A/dm², the hardness value increases with the addition of SDS, due to the surfactant's assistance during the electrodeposition process. However, at 3 A/dm², the hardness values fluctuate with increasing SDS content, likely due to the interaction between the current density and the SDS surfactant. At higher current densities and SDS contents, the deposition rate is higher and more uniform, which contributes to the growth of grain size and coating thickness, both of which significantly influence the hardness value of the composite coatings.

A study by Sabri et al., (2012) mentioned that higher SDS content improves the incorporation of nanoparticles in the composite coatings, leading to higher hardness values due to the increased presence of nano-alumina particles, which have hardening and reinforcing effects. Therefore, the incorporation of nickel-quarry dust particles in the coatings significantly affects the hardness value of the nickel-quarry dust composite coatings.

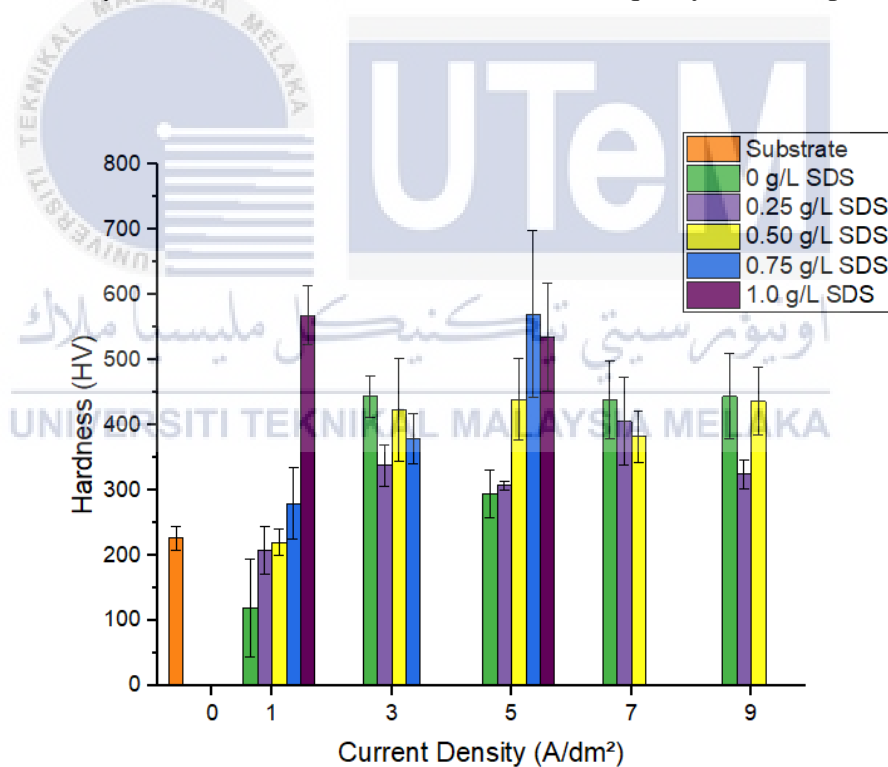
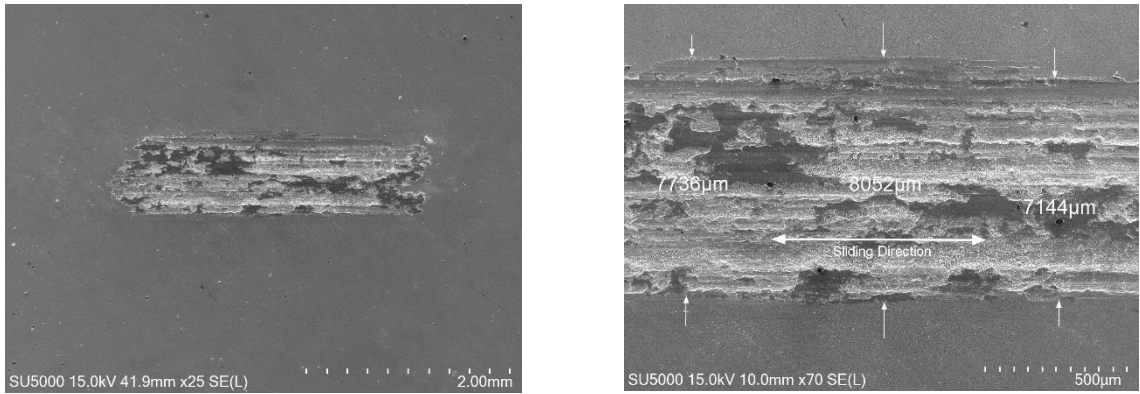


Figure 4.12: Hardness value of nickel-quarry dust composite coatings

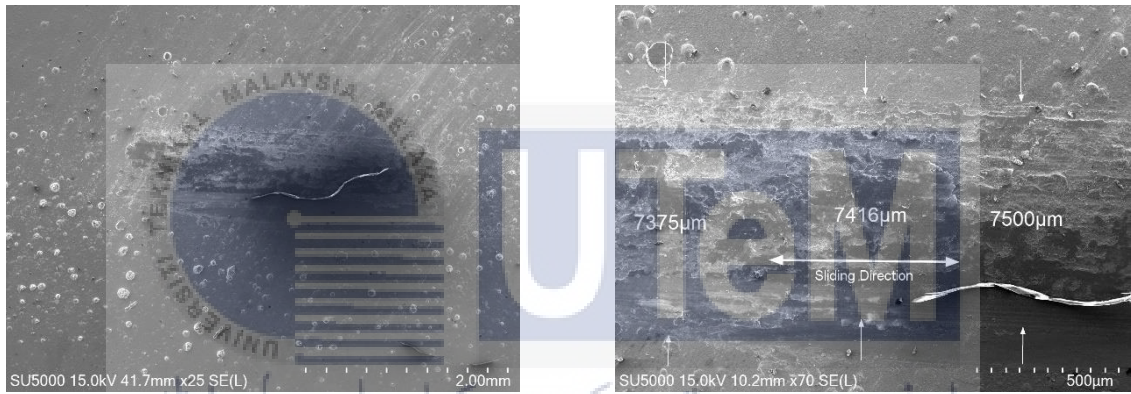
4.4.2 Wear Test on The Nickel-Quarry Dust Composite Coatings

The wear tracks of nickel-quarry dust composite coatings were analyzed using Scanning Electron Microscopy (SEM) to examine the wear behaviour. Figure 4.13 presents three different wear tracks, all with a constant SDS content of 0.50 g/L but varying current densities. As depicted in Figure 4.13, the wear scars on the coatings decrease in width as the current density increases. Specifically, Figure 4.13(a) shows the wear scars at a current density of 1 A/dm² with an average width of 7644 μm. In contrast, Figure 4.13(b) demonstrates a reduced average width of 7430 μm when the current density is increased to 3 A/dm², while maintaining the same SDS content. The wear scars' width further decreases to 6360 μm at a current density of 9 A/dm², as illustrated in Figure 4.13(c). This reduction in scar width is attributed to the higher current density, which facilitates the incorporation of more nickel-quarry dust particles into the coating. The agglomeration of these particles in the nickel-quarry dust composite coatings hinders the formation of wear scars during the wear test conducted using a pin-on-disc machine.

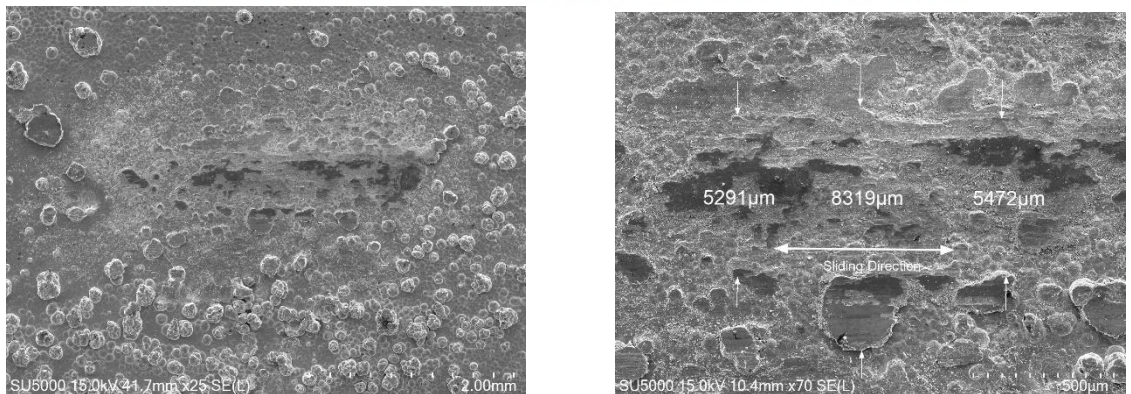
Figure 4.14 illustrates the wear tracks of nickel-quarry dust composite coatings at a current density of 5 A/dm² with varying SDS content. Figure 4.14(a) displays three measurements of coating scars, with an average width of 7168 μm. As the SDS content increases to 0.50 g/L, the average scar width increases to 7430 μm, as shown in Figure 4.14(b). The scar width further increases to an average of 9161 μm as the SDS content reaches 1.0 g/L, as depicted in Figure 4.14(c). This increase in scar width is influenced by the rising SDS content, which facilitates particle distribution and results in a rougher and thicker coating surface. The rougher surface enhances the interaction between the ball and the coating during the wear test, leading to wider scars. The participation of nickel-quarry dust particles, aided by SDS, ensures uniform distribution, contributing to the coating's thickness and roughness. Consequently, as the SDS content increases, the rough coating surface produces wider scars during the wear test due to the intensified reaction between the ball and the rough coating surface.



(a)

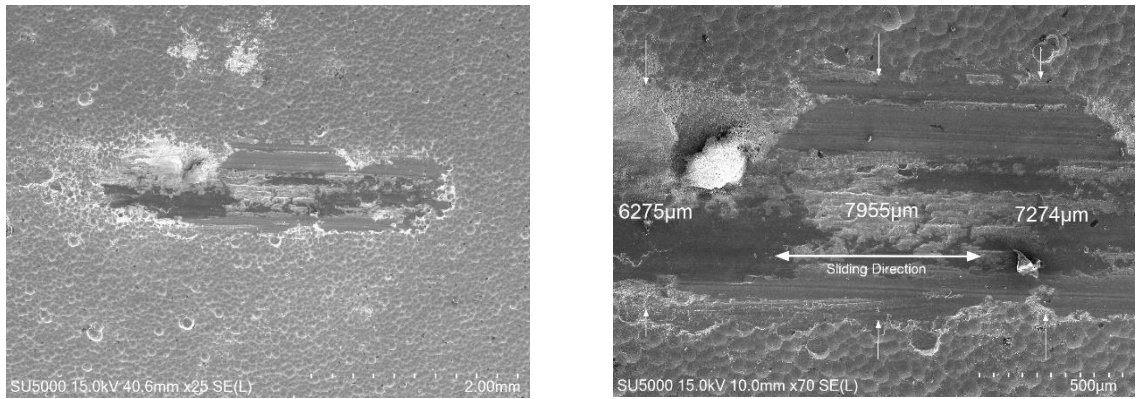


(b)

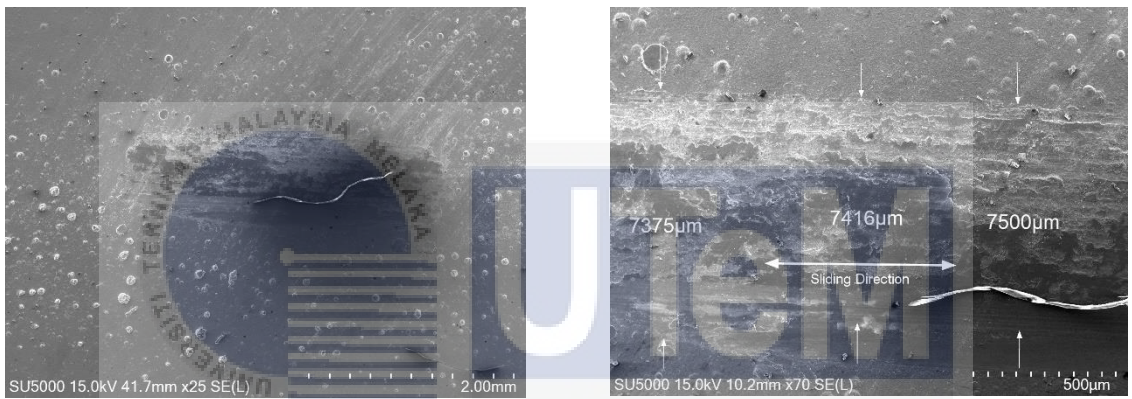


(c)

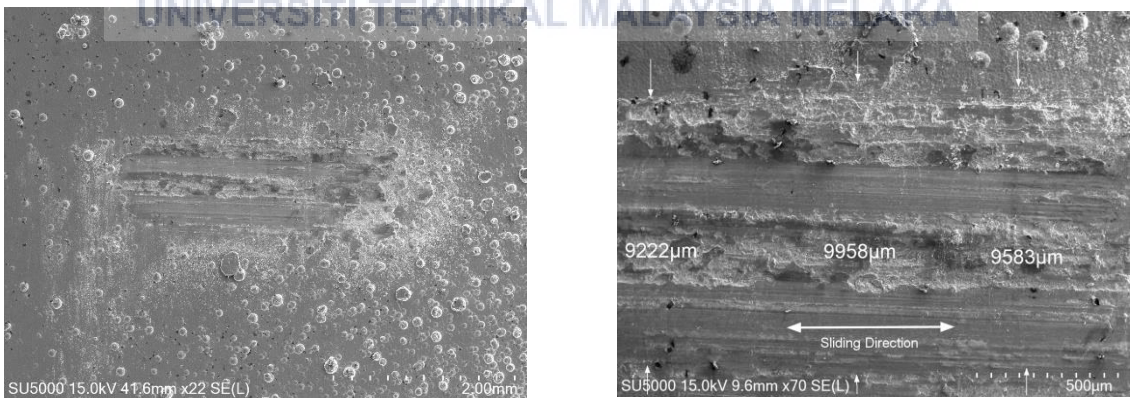
Figure 4.13: Wear track of nickel-quarry dust composite coatings produce using 0.50 g/L SDS at various current density (a) 1 A/dm² (b) 5 A/dm² (c) 9 A/dm²



(a)



(b)



(c)

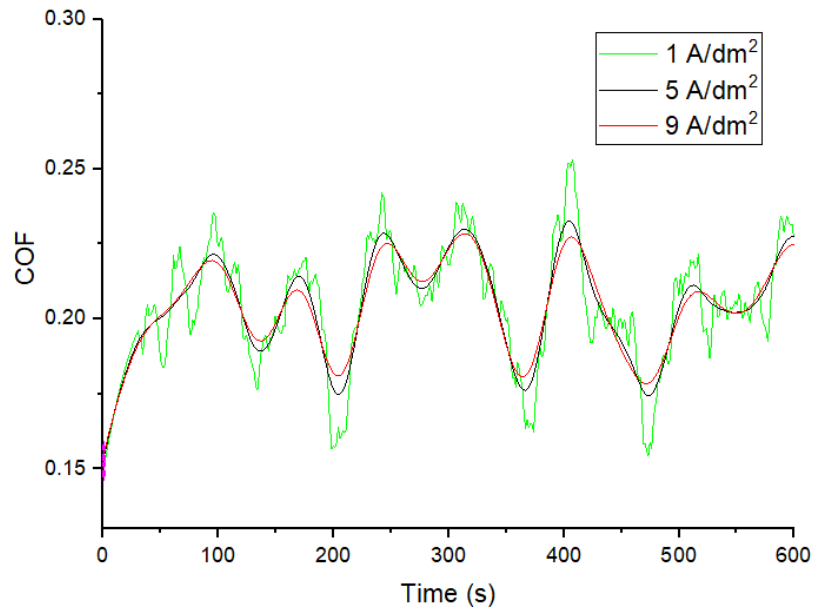
Figure 4.14: Wear track of nickel-quarry dust composite coatings produce at 5 A/dm² of current density with various SDS content at (a) 0 (b) 0.50 (c) 1.0 g/L

4.4.2 Effect of Various Current Density and SDS Content on the Coefficient of Friction (COF)

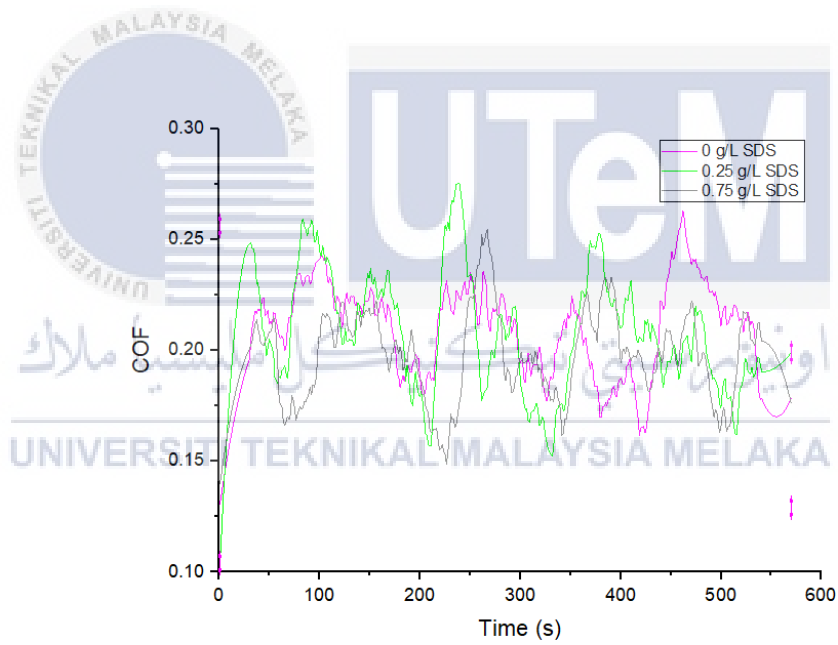
The effect of varying current density and SDS content on the COF is illustrated in Figure 4.15. Figure 4.15(a) depicts the impact of different current densities on the COF at an SDS content of 0.50 g/L. As shown in Figure 4.15(a), the COF decreases as the current density increases. The highest COF value of 0.205 is observed at a current density of 1 A/dm² with 0.50 g/L SDS content. When the current density is increased to 5 A/dm², the average COF value decreases to 0.199. However, as the current density rises to 9 A/dm², the COF value increases again to 0.205, as seen in Figure 4.15(a).

The fluctuating COF values suggest that during the wear test, the test may have been conducted in areas with varying concentrations of nickel-quarry dust particles, leading to inconsistent COF values. The rapid deposition of nickel-quarry dust particles at high current densities during the electrodeposition process could cause non-uniform particle distribution, contributing to these fluctuations.

Figure 4.15(b) illustrates the effect of various SDS content on the COF value at a current density of 1 A/dm². The average COF value without SDS is 0.201, indicating a low COF value due to the absence of a surfactant to aid in particle distribution during the electrodeposition process at low current density. As the SDS content increases to 0.25 g/L, the COF value rises to 0.205, attributed to the presence of the surfactant during deposition. The same average value is observed for SDS content at 0.75 g/L, indicating that the optimal COF value of 0.205 occurs at both 0.25 g/L and 0.75 g/L SDS content. This suggests that the inclusion of SDS during the deposition of nickel-quarry dust particles effectively aids in particle distribution, resulting in higher COF values. A high COF value indicates that the coating surface is rougher and offers greater resistance against sliding motion.



(a)



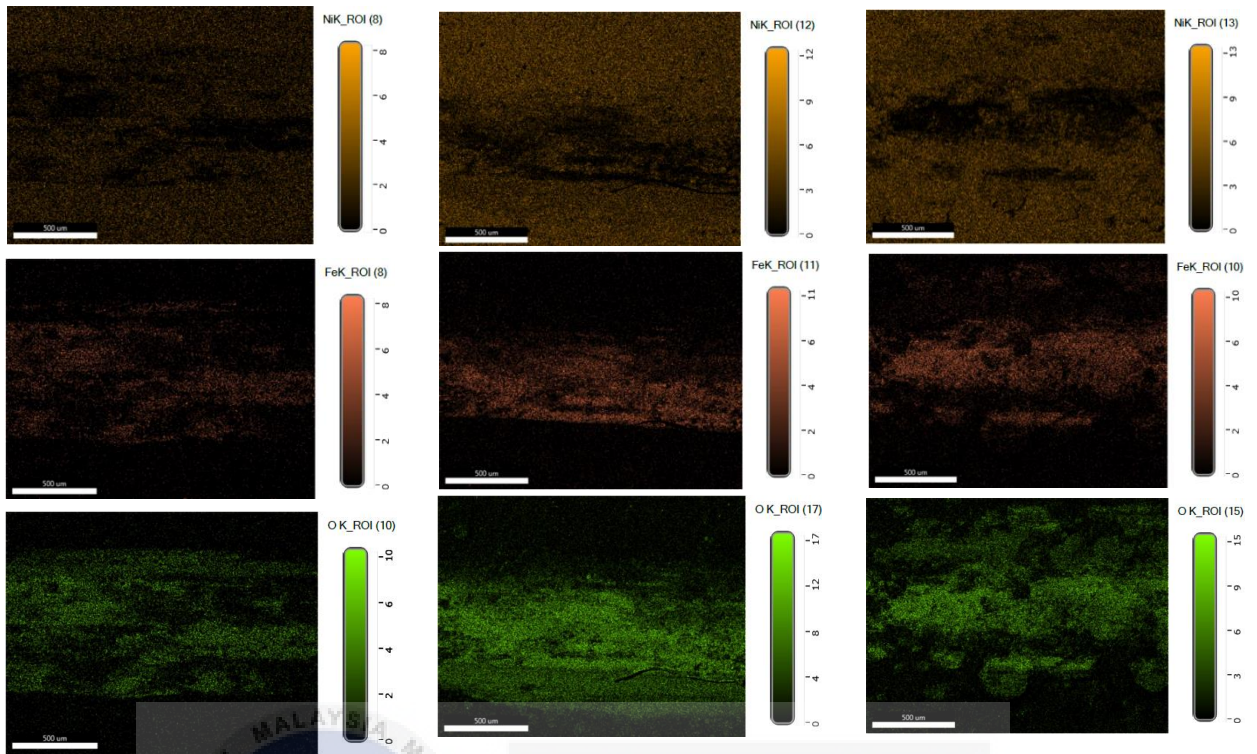
(b)

Figure 4.15: The COF value of at (a) various current density and 0.50 g/L of SDS content (b) various SDS content and 1 A/dm² current density

4.4.3 Energy Dispersive X-ray (EDX) on Wear Track

The wear track of nickel-quarry dust composite coatings has been undergoing Energy Dispersive X-ray (EDX) analysis. Figure 4.16 shows the EDX mapping of coating scars using SEM that shows some worn out element during the wear test. Figure 4.16 (a) shows the EDX mapping on wear track at 0.50 g/L with various current density. As shown in figure 4.16 (a) as the current density increases the worn-out coating are reduced. Based on the figure 4.16 (a) at current density 1 A/dm² there is more iron element if compared to the others current density and the nickel element in the 4.16 (a) mapping shows as the current density increase there is huge amount of nickel elements. This is because of the high deposition rate of nickel-quarry dust particles at high current density that tend the particles to agglomerate and form a thick coating. When the wear test is conducted, at high current density the possibility of coating to worn-out is small because of the thickness of the coating. When the reaction between the ball and coating surface during the wear test it creates iron debris that surrounds the wear track.

Figure 4.17 shows the EDX mapping of the worn-out coating with increasing SDS content. When the coating is deposited without any SDS surfactant, a significant amount of wear is observed, as shown in Figure 4.17 (a). This is due to the low deposition rate of nickel-quarry dust particles on the coating surface and the lack of SDS surfactant to aid in particle dispersion. With the addition of 0.50 g/L SDS surfactant, the amount of worn-out coating is reduced, as depicted in Figure 4.17 (b). This reduction is attributed to the increased coating thickness resulting from better dispersion of nickel-quarry dust particles during the electrodeposition process due to the presence of SDS. The worn-out coating particles are further reduced as the SDS surfactant content is increased to 1.0 g/L, as shown in Figure 4.17 (c). The presence of SDS improves particle distribution, leading to an increase in coating thickness. The enhanced distribution of nickel-quarry dust particles, facilitated by SDS, results in particle agglomeration and stacking, contributing to a thicker coating. Therefore, increasing the SDS content improves the distribution of nickel-quarry dust particles, resulting in a thicker coating and a reduction in worn-out coatings.



(a)

(b)

(c)

Figure 4.16: EDX mapping on wear track of nickel-quarry dust composite coatings produce using 0.50 g/L SDS content with various current density (a) 1 A/dm² (b) 5 A/dm² (c) 9 A/dm²

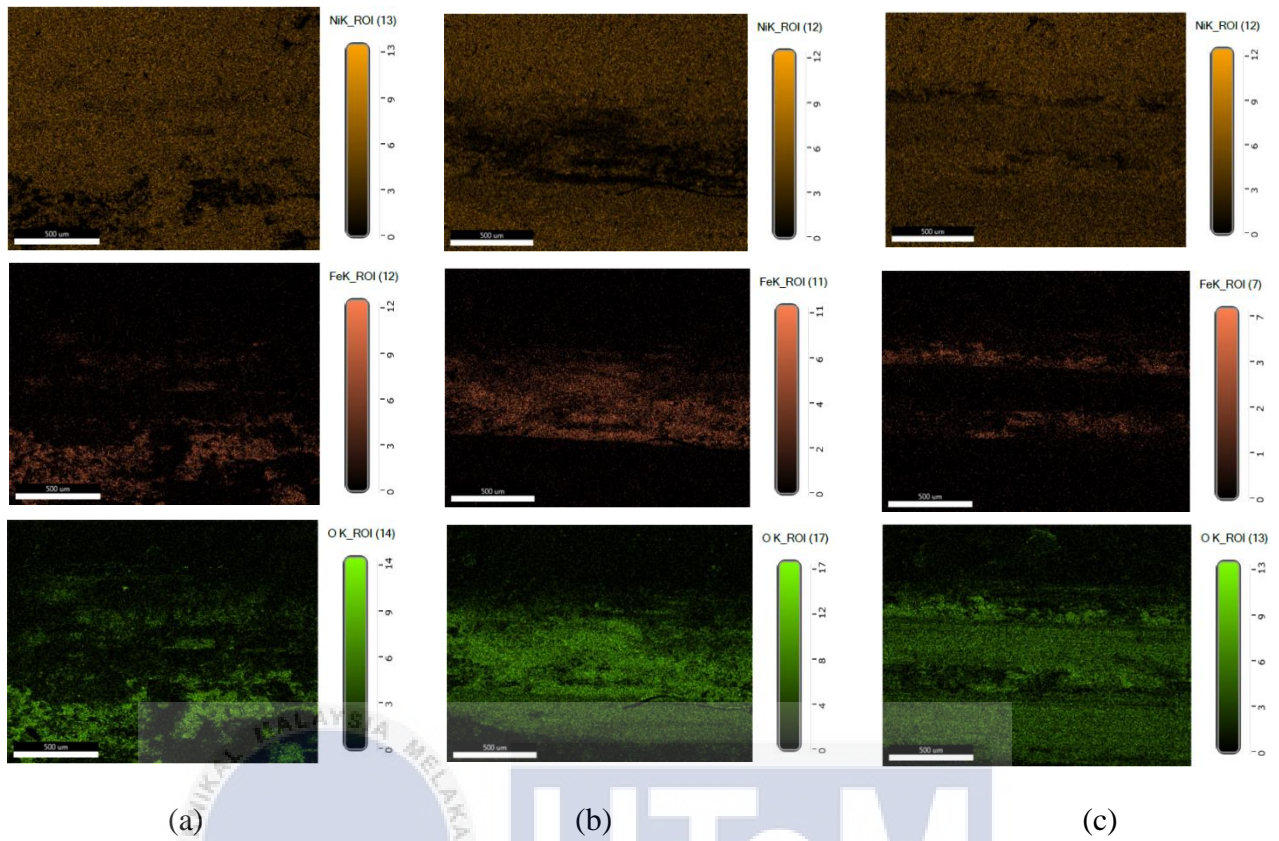


Figure 4.17: EDX mapping on wear track of nickel-quarry dust composite coating produce at 5 A/dm² of current density with various SDS content (a) 0 (b) 0.50 (c) 1.0 g/L

CHAPTER 5

CONCLUSION AND RECOMMENDATION

5.1 Conclusion

Ni-Recycled quarry dust composite coatings are successfully coated with using various current density and SDS content. However, some experimental are failed due to high current density and SDS content that tend to create an overflow of solution during the experimental process. The usage of recycled quarry dust as a substitute element to raw alumina (Al_2O_3) and silica (SiO_2) is an environmentally friendly method. Due to high in alumina and silica, the composite coating consists of nickel and quarry dust give an amazing outcome from the experimental result. The experimental investigation into Ni-recycled quarry dust (QD) composite coatings has provided several important insights:

- 1) As current density increases from 1 A/dm^2 to 9 A/dm^2 , the surface morphology of the Ni-QD composite coatings becomes more agglomerated, compact, and stacked due to the higher deposition rate. This results in a significant difference in the Ni-QD grain structure.
- 2) Increasing the sodium dodecyl sulphate (SDS) content enhances the uniformity and compactness of the Ni-QD grain structure. SDS facilitates uniform distribution of Ni-QD particles, with an optimal concentration identified at 0.50 g/L . Exceeding this SDS content, particularly at high current densities, can lead to solution overflow and experimental failure.
- 3) The wear resistance of Ni-QD composite coatings improves with increasing current density. This improvement is attributed to the thicker coating layers formed at higher current densities, which distribute more particles across the surface, enhancing wear resistance.

- 4) The wear resistance also increases with SDS content up to the optimal value of 0.50 g/L. Uniformly distributed Ni-QD particles result in a thicker and more uniform coating, contributing to better wear properties.
- 5) The hardness of Ni-QD composite coatings increases with current density up to 5 A/dm². Beyond this point, the hardness decreases due to the excessive interaction between high current density and SDS content. The optimal hardness is achieved at a current density of 5 A/dm².
- 6) The hardness of the coatings increases with SDS content up to the optimal value of 0.50 g/L. Beyond this level, the hardness decreases, likely due to excessive SDS interaction with the applied current density, leading to experimental failures. The optimal hardness is recorded at this SDS content.
- 7) The ideal conditions for achieving uniform, compact, and well-stacked Ni-QD composite coatings with excellent wear and hardness properties are identified as a current density of 5 A/dm² and an SDS content of 0.50 g/L. These parameters produce the best combination of surface morphology, wear resistance, and hardness.

5.2 Recommendation

To achieve better and more reliable results in future studies, the following improvements are recommended:

- 1) Determine and use an appropriate amount of SDS to ensure experiments can be conducted without failures due to solution overflow.
- 2) Maintain a consistent stirrer speed during both the experimental process and solution preparation to prevent bubble formation, which could lead to experimental failures.
- 3) Regularly measure the coating thickness to understand how current density and SDS content influence this parameter.
- 4) Conduct corrosion tests to evaluate the corrosion resistance of the Ni-QD composite coatings.

REFERENCES

- Alaneme, K. K., & Bamike, B. J. (2018). Characterization of mechanical and wear properties of aluminium based composites reinforced with quarry dust and silicon carbide. *Ain Shams Engineering Journal*, 9(4), 2815–2821. <https://doi.org/10.1016/j.asej.2017.10.009>
- Alizadeh, M., & Cheshmpish, A. (2019). Electrodeposition of Ni-Mo/Al₂O₃ nano-composite coatings at various deposition current densities. *Applied Surface Science*, 466, 433–440. <https://doi.org/10.1016/j.apsusc.2018.10.073>
- Allahyarzadeh, M. H., Aliofkhazraei, M., Rezvani, A. R., Torabinejad, V., & Sabour Rouhaghdam, A. R. (2016). Ni-W electrodeposited coatings: Characterization, properties and applications. In *Surface and Coatings Technology* (Vol. 307, pp. 978–1010). Elsevier B.V. <https://doi.org/10.1016/j.surfcoat.2016.09.052>
- Anwar, S., Khan, F., Zhang, Y., & Caines, S. (2019). Optimization of zinc-nickel film electrodeposition for better corrosion resistant characteristics. *Canadian Journal of Chemical Engineering*, 97(9), 2426–2439. <https://doi.org/10.1002/cjce.23521>
- Bigos, A., Wolowicz, M., Janusz-Skuza, M., Starowicz, Z., Szczerba, M. J., Bogucki, R., & Beltowska-Lehman, E. (2021). Citrate-based baths for electrodeposition of nanocrystalline nickel coatings with enhanced hardness. In *Journal of Alloys and Compounds* (Vol. 850). Elsevier Ltd. <https://doi.org/10.1016/j.jallcom.2020.156857>
- Boukhouiete, A., Boumendjel, S., & Sobhi, N. E. H. (2021). Effect of current density on the microstructure and morphology of the electrodeposited nickel coatings. *Turkish Journal of Chemistry*, 45(5), 1599–1608. <https://doi.org/10.3906/kim-2102-46>
- Das, S., & Das, S. (2021). Properties for Polymer, Metal and Ceramic Based Composite Materials. In *Encyclopedia of Materials: Composites* (Vol. 2, pp. 815–821). Elsevier. <https://doi.org/10.1016/B978-0-12-803581-8.11897-1>
- Demir, M., Kanca, E., & Karahan, İ. H. (2020). Characterization of electrodeposited Ni–Cr/hBN composite coatings. *Journal of Alloys and Compounds*, 844. <https://doi.org/10.1016/j.jallcom.2020.155511>

- Fadzli, M., & Abdollah, B. (2019). *UNIVERSIT TEKNI-AL MALAYSIA MELAKA ME.org PROCEEDINGS OF MECHANICAL*. www.utm.edu.my/care
- Fotovvati, B., Namdari, N., & Dehghanhadikolaie, A. (2019). On coating techniques for surface protection: A review. In *Journal of Manufacturing and Materials Processing* (Vol. 3, Issue 1). MDPI Multidisciplinary Digital Publishing Institute.
<https://doi.org/10.3390/jmmp3010028>
- Habeeb, H. J., Luaibi, H. M., Dakhil, R. M., Kadhum, A. A. H., Al-Amiery, A. A., & Gaaz, T. S. (2018). Development of new corrosion inhibitor tested on mild steel supported by electrochemical study. *Results in Physics*, 8, 1260–1267.
<https://doi.org/10.1016/j.rinp.2018.02.015>
- Hamidi, N. A., Kamdi, Z., Ainuddin, A. R., Hussin, R., & Ibrahim, S. A. (2021). Effect of Current Density and Bath Temperature to The Corrosion and Wear Behaviour of Tungsten Carbide - Nickel Electrodeposition Coating. *Journal of Physics: Conference Series*, 2129(1). <https://doi.org/10.1088/1742-6596/2129/1/012099>
- Harachai, K., Kothanam, N., Qin, J., Boonyongmaneerat, Y., & Jaroenapibal, P. (2020). Hardness and tribological properties of co-electrodeposited Ni-W-B/B coatings. *Surface and Coatings Technology*, 402.
<https://doi.org/10.1016/j.surfcoat.2020.126313>
- He, T., He, Y., Li, H., Su, Z., Fan, Y., & He, Z. (2018). Fabrication of Ni-W-B4C composite coatings and evaluation of its micro-hardness and corrosion resistance properties. *Ceramics International*, 44(8), 9188–9193.
<https://doi.org/10.1016/j.ceramint.2018.02.128>
- Hoche, H., Pusch, C., & Oechsner, M. (2020). Corrosion and wear protection of mild steel substrates by innovative PVD coatings. *Surface and Coatings Technology*, 391.
<https://doi.org/10.1016/j.surfcoat.2020.125659>
- Isern, L., Impey, S., Milosevic, D., Clouser, S. J., & Endrino, J. L. (2024). Wear-resistant nickel-matrix composite coatings incorporating hard chromium carbide particles. *Frontiers in Coatings, Dyes and Interface Engineering*, 1.
<https://doi.org/10.3389/frcdi.2023.1278575>

- Jiang, W., Shen, L., Qiu, M., Wang, X., Fan, M., & Tian, Z. (2018). Preparation of Ni-SiC composite coatings by magnetic field-enhanced jet electrodeposition. *Journal of Alloys and Compounds*, 762, 115–124. <https://doi.org/10.1016/j.jallcom.2018.05.097>
- Kannan, P. K., Chaudhari, S., & Dey, S. R. (2019). Progress in Development of CZTS for Solar Photovoltaics Applications. In *Reference Module in Materials Science and Materials Engineering*. Elsevier. <https://doi.org/10.1016/b978-0-12-803581-8.10502-8>
- Karimzadeh, A., Aliofkhazraei, M., & Walsh, F. C. (2019). A review of electrodeposited Ni-Co alloy and composite coatings: Microstructure, properties and applications. In *Surface and Coatings Technology* (Vol. 372, pp. 463–498). Elsevier B.V. <https://doi.org/10.1016/j.surfcoat.2019.04.079>
- Khodair, Z. T., Khadom, A. A., & Jasim, H. A. (2019). Corrosion protection of mild steel in different aqueous media via epoxy/nanomaterial coating: Preparation, characterization and mathematical views. *Journal of Materials Research and Technology*, 8(1), 424–435. <https://doi.org/10.1016/j.jmrt.2018.03.003>
- Kolle, M. K., Shajahan, S., & Basu, A. (2020). Effect of Electrodeposition Current and Pulse Parameter on Surface Mechanical and Electrochemical Behavior of Ni–W Alloy Coatings. *Metallurgical and Materials Transactions A: Physical Metallurgy and Materials Science*, 51(7), 3721–3731. <https://doi.org/10.1007/s11661-020-05787-0>
- Kul, M., Oskay, K. O., Erden, F., Akça, E., Katirci, R., Köksal, E., & Akinci, E. (2020). Effect of process parameters on the electrodeposition of zinc on 1010 Steel: Central composite design optimization. *International Journal of Electrochemical Science*, 15, 9779–9795. <https://doi.org/10.20964/2020.10.19>
- Lekka, M. (2018). Electrochemical deposition of composite coatings. In *Encyclopedia of Interfacial Chemistry: Surface Science and Electrochemistry* (pp. 54–67). Elsevier. <https://doi.org/10.1016/B978-0-12-409547-2.11716-0>
- Lelevic, A., & Walsh, F. C. (2019). Electrodeposition of Ni[sbnd]P alloy coatings: A review. In *Surface and Coatings Technology* (Vol. 369, pp. 198–220). Elsevier B.V. <https://doi.org/10.1016/j.surfcoat.2019.03.055>

- Li, B., Zhang, W., Zhang, W., & Huan, Y. (2017). Preparation of Ni-W/SiC nanocomposite coatings by electrochemical deposition. *Journal of Alloys and Compounds*, 702, 38–50. <https://doi.org/10.1016/j.jallcom.2017.01.239>
- Li, D., Li, B., Du, S., & Zhang, W. (2019). Synthesis of a novel Ni-B/YSZ metal-ceramic composite coating via single-step electrodeposition at different current density. *Ceramics International*, 45(18), 24884–24893. <https://doi.org/10.1016/j.ceramint.2019.09.121>
- Li, L., Li, C.-Q., & Mahmoodian, M. (2018). *Effect of Applied Stress on Corrosion and Mechanical Properties of Mild Steel*. [https://doi.org/10.1061/\(ASCE\)MT.1943](https://doi.org/10.1061/(ASCE)MT.1943)
- Li, X., Shen, Q., Zhang, Y., Wang, L., & Nie, C. (2021). Wear behavior of electrodeposited nickel/graphene composite coating. *Diamond and Related Materials*, 119. <https://doi.org/10.1016/j.diamond.2021.108589>
- Mersagh Dezfuli, S., & Sabzi, M. (2019). Deposition of ceramic nanocomposite coatings by electroplating process: A review of layer-deposition mechanisms and effective parameters on the formation of the coating. *Ceramics International*, 45(17), 21835–21842. <https://doi.org/10.1016/j.ceramint.2019.07.190>
- Mousavi, R., Bahrololoom, M. E., & Deflorian, F. (2019). The effect of surfactant on the microstructure and corrosion resistance of electrodeposited Ni-Mo alloy coatings. *Anti-Corrosion Methods and Materials*, 66(5), 631–637. <https://doi.org/10.1108/ACMM-03-2019-2087>
- Natarajan, J., Yang, C. H., & Karuppasamy, S. S. (2021). Investigation on microstructure, nanohardness and corrosion response of laser clad colmonoy-6 particles on 316l steel substrate. *Materials*, 14(20). <https://doi.org/10.3390/ma14206183>
- Oliveira, J. A. M., de Almeida, A. F., Campos, A. R. N., Prasad, S., Alves, J. J. N., & de Santana, R. A. C. (2021). Effect of current density, temperature and bath pH on properties of Ni-W-Co alloys obtained by electrodeposition. *Journal of Alloys and Compounds*, 853. <https://doi.org/10.1016/j.jallcom.2020.157104>
- Othman, I. S., Azam, M. A. F. M. M., Bakar, M. F. A., Kasim, M. S., Rahman, T. A., & Mohamad, M. R. (2019). Influence of ball milling duration of quarry dust on the properties of nickel-quarry dust composite coating. *Journal of Mechanical*

Engineering and Sciences, 13(3), 5441–5454.

<https://doi.org/10.15282/jmes.13.3.2019.15.0441>

Parhizkar, N., Ramezanzadeh, B., & Shahrabi, T. (2018). Corrosion protection and adhesion properties of the epoxy coating applied on the steel substrate pre-treated by a sol-gel based silane coating filled with amino and isocyanate silane functionalized graphene oxide nanosheets. *Applied Surface Science*, 439, 45–59.

<https://doi.org/10.1016/j.apsusc.2017.12.240>

Puspitasari, W. C., Ahmad, F., Ullah, S., Hussain, P., Megat-Yusoff, P. S. M., & Masset, P. J. (2019). The study of adhesion between steel substrate, primer, and char of intumescent fire retardant coating. *Progress in Organic Coatings*, 127, 181–193.

<https://doi.org/10.1016/j.porgcoat.2018.11.015>

Rajak, D. K., Pagar, D. D., Kumar, R., & Pruncu, C. I. (2019). Recent progress of reinforcement materials: A comprehensive overview of composite materials. *Journal of Materials Research and Technology*, 8(6), 6354–6374.

<https://doi.org/10.1016/j.jmrt.2019.09.068>

Rosyidan, C., Kurniawan, B., Soegijono, B., Putra, V. G. V., Munazat, D. R., & Susetyo, F. B. (2024). Effect of Current Density on Magnetic and Hardness Properties of Ni-Cu Alloy Coated on Al via Electrodeposition. *International Journal of Engineering, Transactions A: Basics*, 37(2), 213–223. <https://doi.org/10.5829/ije.2024.37.02b.01>

Sabri, M., Sarabi, A. A., & Naseri Kondelo, S. M. (2012a). The effect of sodium dodecyl sulfate surfactant on the electrodeposition of Ni-alumina composite coatings.

Materials Chemistry and Physics, 136(2–3), 566–569.

<https://doi.org/10.1016/j.matchemphys.2012.07.027>

Sabri, M., Sarabi, A. A., & Naseri Kondelo, S. M. (2012b). The effect of sodium dodecyl sulfate surfactant on the electrodeposition of Ni-alumina composite coatings.

Materials Chemistry and Physics, 136(2–3), 566–569.

<https://doi.org/10.1016/j.matchemphys.2012.07.027>

Sajjadnejad, M., Haghshenas, S. M. S., Badr, P., Setoudeh, N., & Hosseinpour, S. (2021). Wear and tribological characterization of nickel matrix electrodeposited composites: A review. In *Wear* (Vols. 486–487). Elsevier Ltd.

<https://doi.org/10.1016/j.wear.2021.204098>

- Sharhida Othman, I., Ammar Farhan Maula Mohd Azam, M., Shafie, M., Shahir Kasim, M., Ahsan, Q., Mohamad Juoi, J., Azwan Sundi, S., Kejuruteraan Pembuatan, F., Teknikal Malaysia Melaka, U., Tuah Jaya, H., Tunggal, D., & Teknologi Kejuruteraan Mekanikal dan Pembuatan, F. (2020). *Influence of saccharin content on the characteristics and hardness properties of electrodeposited nickel-quarry dust composite coatings*.
- Shen, L., Fan, M., Qiu, M., Jiang, W., & Wang, Z. (2019). Superhydrophobic nickel coating fabricated by scanning electrodeposition. *Applied Surface Science*, 483, 706–712. <https://doi.org/10.1016/j.apsusc.2019.04.019>
- Shrivastava, S., Rajak, D. K., Joshi, T., Singh, D. K., & Mondal, D. P. (2024). Ceramic Matrix Composites: Classifications, Manufacturing, Properties, and Applications. *Ceramics*, 7(2), 652–679. <https://doi.org/10.3390/ceramics7020043>
- Singh, G., Vasudev, H., Bansal, A., Vardhan, S., & Sharma, S. (2020). Microwave cladding of Inconel-625 on mild steel substrate for corrosion protection. *Materials Research Express*, 7(2). <https://doi.org/10.1088/2053-1591/ab6fa3>
- Suleiman, R. K., Kumar, A. M., Adesina, A. Y., Al-Badour, F. A., Meliani, M. H., & Saleh, T. A. (2020). Hybrid Organosilicon-Metal oxide Composites and their Corrosion Protection Performance for Mild Steel in 3.5% NaCl Solution. *Corrosion Science*, 169. <https://doi.org/10.1016/j.corsci.2020.108637>
- Sun, J., Ye, D., Zou, J., Chen, X., Wang, Y., Yuan, J., Liang, H., Qu, H., Binner, J., & Bai, J. (2023). A review on additive manufacturing of ceramic matrix composites. In *Journal of Materials Science and Technology* (Vol. 138, pp. 1–16). Chinese Society of Metals. <https://doi.org/10.1016/j.jmst.2022.06.039>
- Sunday Isaac Fayomi, O., & Patricia Idowu Popoola, A. (2019). Corrosion propagation challenges of mild steel in industrial operations and response to problem definition. *Journal of Physics: Conference Series*, 1378(2). <https://doi.org/10.1088/1742-6596/1378/2/022006>
- Szala, M., Walczak, M., Pasierbiewicz, K., & Kamiński, M. (2019). Cavitation erosion and slidingwear mechanisms of AlTiN and TiAlN films deposited on stainless steel substrate. *Coatings*, 9(5). <https://doi.org/10.3390/COATINGS9050340>

- Tan, S., Algül, H., Kiliçaslan, E., Alp, A., Akbulut, H., & Uysal, M. (2023). The effect of ultrasonic power on high temperature wear and corrosion resistance for Ni based alloy composite coatings. *Colloids and Surfaces A: Physicochemical and Engineering Aspects*, 656. <https://doi.org/10.1016/j.colsurfa.2022.130345>
- Walsh, F. C., Wang, S., & Zhou, N. (2020). The electrodeposition of composite coatings: Diversity, applications and challenges. In *Current Opinion in Electrochemistry* (Vol. 20, pp. 8–19). Elsevier B.V. <https://doi.org/10.1016/j.coelec.2020.01.011>
- Wasekar, N. P., Bathini, L., Ramakrishna, L., Rao, D. S., & Padmanabham, G. (2020). Pulsed electrodeposition, mechanical properties and wear mechanism in Ni-W/SiC nanocomposite coatings used for automotive applications. *Applied Surface Science*, 527. <https://doi.org/10.1016/j.apsusc.2020.146896>
- Wu, C., Xu, F., Wang, H., Liu, H., Yan, F., & Ma, C. (2023). Manufacturing Technologies of Polymer Composites—A Review. In *Polymers* (Vol. 15, Issue 3). MDPI. <https://doi.org/10.3390/polym15030712>
- Wu, W., Huang, J., Näther, J., Omar, N. A. B., Köster, F., Lampke, T., Liu, Y., Pan, H., & Zhang, Y. (2021). Texture orientation, morphology and performance of nanocrystalline nickel coatings electrodeposited from a Watts-type bath: Effects of H₃BO₃ concentration and plating time. *Surface and Coatings Technology*, 424. <https://doi.org/10.1016/j.surfcoat.2021.127648>
- Yamamoto, T., Igawa, K., Tang, H., Chen, C. Y., Chang, T. F. M., Nagoshi, T., Kudo, O., Maeda, R., & Sone, M. (2019). Effects of current density on mechanical properties of electroplated nickel with high speed sulfamate bath. *Microelectronic Engineering*, 213, 18–23. <https://doi.org/10.1016/j.mee.2019.04.012>
- Yang, Z., Liu, X., & Tian, Y. (2019). Fabrication of super-hydrophobic nickel film on copper substrate with improved corrosion inhibition by electrodeposition process. *Colloids and Surfaces A: Physicochemical and Engineering Aspects*, 560, 205–212. <https://doi.org/10.1016/j.colsurfa.2018.10.024>
- Yap, C. Y., Liew, P. J., & Yan, J. (2020). Surface modification of tungsten carbide cobalt by electrical discharge coating with quarry dust suspension. *International Journal of Advanced Manufacturing Technology*, 111(7–8), 2105–2116. <https://doi.org/10.1007/s00170-020-06268-9>

- Yasin, G., Arif, M., Nizam, M. N., Shakeel, M., Khan, M. A., Khan, W. Q., Hassan, T. M., Abbas, Z., Farahbakhsh, I., & Zuo, Y. (2018). Effect of surfactant concentration in electrolyte on the fabrication and properties of nickel-graphene nanocomposite coating synthesized by electrochemical co-deposition. *RSC Advances*, 8(36), 20039–20047. <https://doi.org/10.1039/c7ra13651j>
- Zhang, F., Yao, Z., Moliar, O., Tao, X., & Yang, C. (2020). Nanocrystalline Ni coating prepared by a novel electrodeposition. *Journal of Alloys and Compounds*, 830. <https://doi.org/10.1016/j.jallcom.2020.153785>
- Zhang, H., Zhang, N., & Fang, F. (2020). Fabrication of high-performance nickel/graphene oxide composite coatings using ultrasonic-assisted electrodeposition. *Ultrasonics Sonochemistry*, 62. <https://doi.org/10.1016/j.ultsonch.2019.104858>
- Zhang, P., Zhao, Y., Huang, J., Li, J., Cao, L., Liu, J., Han, G., Du, W., Chen, L., Xiao, L., Wang, Q., Yang, Y., Zhu, S., & Li, W. (2023). Enhanced mechanical and wear properties of Ni-W-SiC composite coatings by synergistic influence of micro-nano SiC mixture. *Surface and Coatings Technology*, 467. <https://doi.org/10.1016/j.surfcoat.2023.129678>
- Zhang, Q., Yang, Y., Ren, X. xing, Yang, Z. long, Gao, P. yue, Zhao, C. ce, Chu, Z. hua, Wang, L., Li, J., & Dong, Y. chun. (2018). Microstructure and properties of composite coatings prepared by plasma spraying ZrO₂-B₂O₃-Al composite powders. *Journal of Alloys and Compounds*, 740, 124–131. <https://doi.org/10.1016/j.jallcom.2017.12.335>
- Zhang, X. H., Li, X. X., Liu, W. J., Fan, Y. Q., Chen, H., & Liang, T. X. (2019). Preparation and tribological behavior of electrodeposited Ni–W–GO composite coatings. *Rare Metals*, 38(7), 695–703. <https://doi.org/10.1007/s12598-018-1173-0>
- Zhou, S., Xu, Y., Liao, B., Sun, Y., Dai, X., Yang, J., & Li, Z. (2018). Effect of laser remelting on microstructure and properties of WC reinforced Fe-based amorphous composite coatings by laser cladding. *Optics and Laser Technology*, 103, 8–16. <https://doi.org/10.1016/j.optlastec.2018.01.024>
- Zolfaghari, M., Arab, A., & Asghari, A. (2019). Surfactant-Assisted Electrodeposition of Nickel Nanostructures and Their Electrocatalytic Activities Toward Oxidation of

Sodium Borohydride, Ethanol, and Methanol. *ChemistrySelect*, 4(15), 4487–4495.

<https://doi.org/10.1002/slct.201900345>



APPENDICES

GANTT CHART PSM I

Activities	Weeks														
	1	2	3	4	5	6	7	8	9	10	11	12	13	14	15
Title Selection & 1st Meeting with Supervisor															
a) FYP I title selection															
b) 1 st Meeting with supervisor															
Chapter 1															
a) Introduction															
a) 2 nd Meeting with supervisor															
b) Chapter 1 submission to supervisor															
Chapter 2															

a) Meeting with supervisor																			
b) Submission of chapter 2																			
Chapter 3																			
a) Meeting with supervisor																			
b) Submission of Chapter 3																			
Poster Presentation																			
a) Mock presentation																			
b) Poster Presentation																			
Submission / Important Deadline																			
a) Logbook																			
b) FYP Report																			

Gantt Chart PSM II

Activities	Weeks														
	1	2	3	4	5	6	7	8	9	10	11	12	13	14	15
Sample Preparation															
c) Grinding & Polishing															
d) Roughness test															
Quarry Dust Preparation															
c) Ball Milling															
d) Sieving Process															
e) PSA Analysis															
Solution Preparation															
c) Watts Bath Preparation in Bulk															
Experimentation															

Characterization of Coatings																				
c) SEM Analysis																				
d) XRD Analysis																				
Mechanical Testing																				
c) Hardness Test																				
d) Wear Test																				
e) Corrosion Test																				
Report Writing																				
a) Result of Experiment																				
b) Discussion																				
Submission / Important Deadline																				
c) Logbook																				
d) FYP Presentation																				
e) FYP Report																				